FIRST PRINCIPLES APPROACH TO IDENTIFICATION OF POTENTIAL FERROELECTRIC AND MULTIFERROIC MOLECULAR MATERIALS

A Thesis
Presented to
The Academic Faculty

by

Brandon Plaisance

In Partial Fulfillment
of the Requirements for the Degree
Master of Science in the
School of Chemical and Biomolecular Engineering

Georgia Institute of Technology

May 2016

FIRST PRINCIPLES APPROACH TO IDENTIFICATION OF POTENTIAL FERROELECTRIC AND MULTIFERROIC MOLECULAR MATERIALS

Approved by:

Dr. David S. Sholl, Advisor
School of Chemical and Biomolecular Engineering
Georgia Institute of Technology

Dr. Krista S. Walton
School of Chemical and Biomolecular Engineering
Georgia Institute of Technology

Dr. Martin Maldovan
School of Chemical and Biomolecular Engineering
Georgia Institute of Technology

Date Approved: April 22, 2016

In nomine Patris, et Filii, et Spiritus Sancti

ACKNOWLEDGEMENTS

TABLE OF CONTENTS

LIST OF TABLES

LIST OF FIGURES

LIST OF SYMBOLS AND ABBREVIATIONS

P_s	Total Spontaneous Polarization
P_{elec}	Electronic Contribution to the Spontaneous Polarization
P_{ion}	Ionic Contribution to the Spontaneous Polarization
p	Dipole Moment
V	Volume
MOF	Metal-Organic Framework
CoRE	Computational-Ready Experimental
CSD	Cambridge Structural Database
DFT	Density Functional Theory
VASP	Vienna Ab-initio Simulation Package
PBE	Perdew-Burke-Ernzerhof
PAW	Projector-Augmented Wave
GGA	Generalized Gradient Approximation
NEB	Nudged Elastic Band
MEP	Minimum Energy Pathway
cNEB	Climbing Nudged Elastic Band
BTO	Barium Titanate ($BaTiO_3$)
SNW	Sandwich Nanowires

SUMMARY

Flexible electronics have garnered much interest over the past several decades. Hybrid organic-inorganic materials, such as metal-organic frameworks, offer a unique opportunity to encompass the effective electronic properties of the inorganic material and the flexible nature of the organic with the potential of enhancing other desirable properties, such as the contributing multiferroicity. Using a first principles approach, the goal of this thesis is to serve as a guide for identifying potential ferroelectric and multiferroic metal-organic frameworks. This is done through a screening method of metal-organic frameworks based on their geometry; certain symmetry operators cannot be present in a ferroelectric material. We report the theoretical spontaneous polarization for several dozens of MOFs in which ferroelectricity has not previously been tested, and further we discuss the likelihood that these materials could be engineered to have either increased polarization or added ferromagnetism, the latter of which would lead to multiferroicity.

CHAPTER 1

INTRODUCTION

Flexible electronics have garnered much interest over the past several decades[1]. One of

several important thrusts in developing this discipline is identifying storage, sensing, and

energy harvesting materials which still perform under strains and stresses, which many of

the current brittle materials used for these applications do not do well. Hybrid materials,

such as metal-organic frameworks, offer a unique opportunity to encompass the effective

electronic properties of the inorganic material and the flexible nature of the organic with

the potential of enhancing other desirable properties, such as the contributing

multiferroicity. Using a first principles approach, the goal of this thesis is to serve as a

guide for identifying potential ferroelectric or multiferroic metal-organic frameworks.

1.1 FERROELECTRICITY AND MULTIFERROICITY IN MATERIALS

1.1.1 Ferromagnetism

To understand the mechanism behind ferroelectricity and multiferroicity, it is prudent to

revisit the primary ferroic order with which most are more familiar: ferromagnetism. A

material is said to be ferromagnetic if: 1) a spontaneous magnetic moment is created in

the material by exposing it to an external magnetic field and 2) this magnetic moment can

be switched by reversing the external field[2]. In general, magnetism is caused by the

quantum mechanical spin of electrons in the material. Materials which align these spins
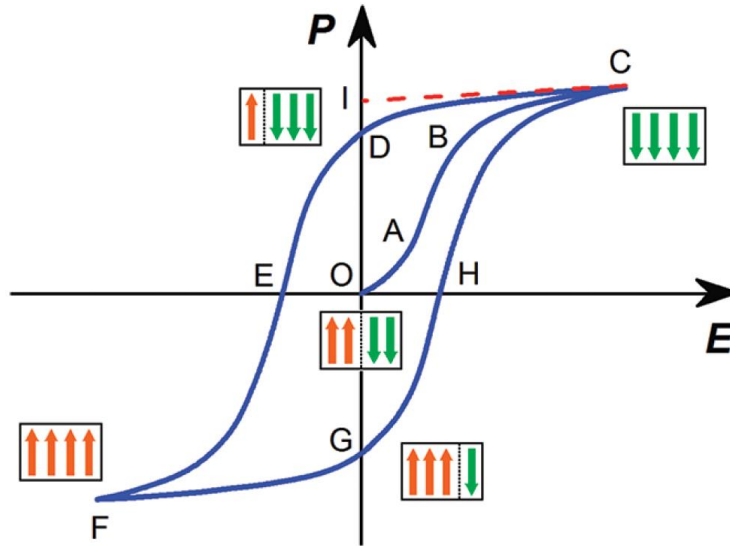
Figure 1 *Example of an electric hysteresis loop from Ref [3]. Polarization (P) vs applied electric field (E) is mapped, and illustrations of sample domains are shown at various portions of the path, which starts at the origin (O) and follows A-H. I represents the value of spontaneous polarization.*

across large domains in response to external magnetic fields are said to be ferromagnetic. The most common examples of ferromagnetic materials are transition metals which have partially filled electron shells—such as iron, cobalt, and nickel—but there are also examples of organic compounds with these properties[4]. Current technologies which use ferromagnetic materials include electric motors, generators, and magnetic storage devices such as hard disks.

1.1.2   Ferroelectricity

The second most commonly studied primary ferroic order is ferroelectricity. Similar to the mechanism for ferromagnetism, ferroelectricity is realized in a material when an external electric field creates a spontaneous polarization, which is an alignment of dipole
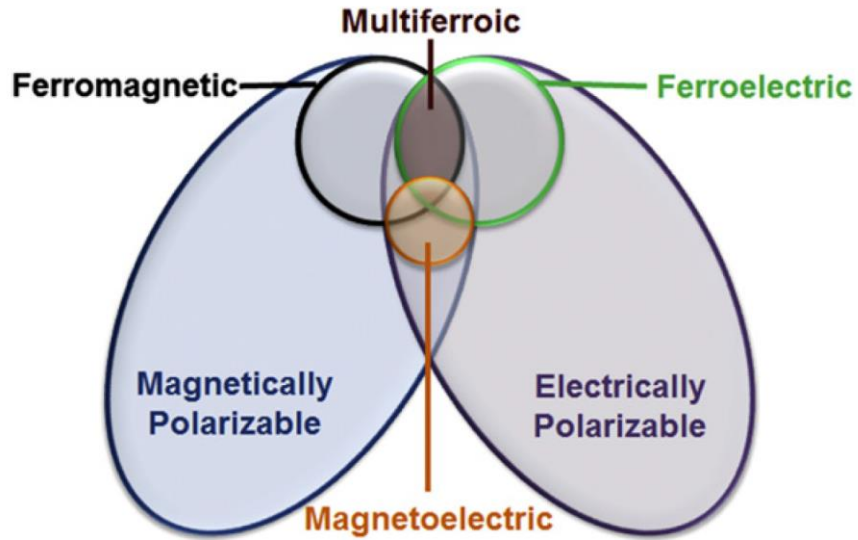
Figure 2 *Relationship between ferromagnetic, ferroelectric, and multiferroic materials from Refs. [5, 6].*

moments across a particular volume of the material[7]. Dipole moments in a material can come from two sources: the orientation of nuclei relative to each other and the orientation of the electron density to a given reference point. This distinction between the types of dipole moment determination can lead to issues in ensuring the calculation of dipole moments is correct, a topic we return to in subsequent sections. When the dipole moments align across large domains, the material is considered ferroelectric. An example of the typical test for polarization switching is a hysteresis loop, shown in Figure 1. The most commonly utilized materials with the ability to switch polarization are metal oxides of the perovskite family such as barium titanate[8], lead zirconate titanate[9, 10], and lithium niobate[11-15]. The most important applications for ferroelectric materials include data storage, sensing, energy harvesting and electro-optic devices.

3

1.1.3 Multiferroicity

When any combination of the primary ferroic orders exists within the same material, it is said the material displays multiferroic properties. The relationship between ferroelectricity and ferromagnetism in terms of multiferroicity is shown in Figure 2. Along with the above mentioned primary ferroic orders, two others also exist[16], ferroelasticity and ferrotoroidicity, which are only included here for completeness and are not investigated in the scope of this thesis. Although multiferroic materials are known to exist, this property is not utilized in any current applications. It is predicted that multiferroicity could be utilized in high sensitivity magnetic field sensors[5], multiple state memory elements[5, 17], and electrically tunable spin valves[5].

1.2 METAL-ORGANIC FRAMEWORKS

1.2.1 What are metal-organic frameworks?

Metal-organic frameworks (MOFs) are crystalline nanoporous materials which typically feature metal centers, or nodes, and organic molecules as linkers forming a 2- or 3-dimensional network. Several properties of MOFs—including the hybrid inorganic-organic nature, their flexibility, and their absorption abilities—make them attractive materials for various applications, such as gas storage[18], molecular sieving[19], and catalysis[20]. Given the multitude of combinations of compounds which constitute this class of materials and the range of potential applications of interest, computational screening methods can play an important role in identifying potential candidates. To assist with these screening methods, several databases of MOFs exist. Among the most useful of these are ones which are prescreened to only include experimental realized MOFs, such as the Computationally-Ready Experimental (CoRE) MOF Database[21],

which uses a subclass from the Cambridge Structural Database (CSD) of existing and verified MOFs which have well-defined and porous structures.

1.2.2 Origins of ferroelectricity

One of the interesting aspects of the field of ferroelectric materials is that although it is dominated by inorganic systems, the first reported detection of this property was found in a hybrid inorganic-organic material. Potassium sodium tartrate tetrahydrate, $[KNa(C_4H_4O_6)] \cdot 4H_2O$, commonly known as Rochelle salt, was first discovered to have polarization of a hysteretic nature in 1920 by Joseph Valasek[22]. The spontaneous polarization of this particular material was found to be 0.25 $\mu C \cdot cm^{-2}$ [3], which is substantially lower than the spontaneous polarization in barium titanate (26 $\mu C \cdot cm^{-2}$) [23].

1.3 CHARACTERIZED FERROELECTRIC MOFS

There are several examples of metal-organic frameworks which show varying degrees of success in demonstrating ferroelectric properties[3]. In this brief survey of some of the typical ferroelectric MOFs, the structures will be categorized by the organic part. This is done because often the switchable dipole moment within the material occurs in this organic part as opposed to the inorganic metal nodes.

1.3.1 Formate family

The formate anion ($HCOO^-$) is a versatile organic ligand which allows for several different bridging modes: monodentate, bidentate, tridentate, and tetradentate[24]. It is the simplest carboxylate ligand, and is present in many magnetic MOFs because its short length does not interfere with internal magnetic interactions necessary in magnetic

materials [25]. Copper (II) formate tetrahydrate, $[Cu(HCOO)_2(H_2O)_2] \cdot 2H_2O$, is one such material [26]. It undergoes an antiferroelectric-paraelectric transition at approximately 235 K. Another example of a magnetic MOF featuring the formate anion is $[Mn_3(HCOO)_6] \cdot X$, where X can be any of an assortment of guest molecules which all effect the critical temperature of magnetization in the material. When X = ethanol, this material exhibits a paraelectric-ferroelectric transition near 165 K, and it is believed that the response of polarization is a direct result of this guest molecule and its interaction with the host lattice [27]. A related MOF of the formate family is $[(CH_3)_2NH_2][M(HCOO)_3]$ which utilizes divalent metal centers (M = Mn, Fe, Co, Ni, Zn) to create a perovskite-like structure, typical of inorganic ferroelectric materials [28, 29]. In a related MOF, dimethylammonium is replaced with ethyl ammonium, $CH_3CH_2NH_3^+$ [30], which provides a larger dipole moment and is covered in more detail in subsequent chapters.

1.3.2 Tartrate family

The tartrate anion $(C_4H_4O_6^{-2})$ bonds to metal centers similarly to how the formate anion does, but tartrate is more massive than formate, which hinders some of these MOFs' potential magnetic properties. The classic example of a tartrate MOF was the first discovered ferroelectric, Rochelle salt, discussed previously. Also in the tartrate family is lithium ammonium tartrate monohydrate, $[(NH_4)Li(C_4H_4O_6)] \cdot H_2O$, shows a paraelectric-ferroelectric transition at 106 K [31].

1.3.3 Amino acid family

Of the 20 amino acids, compounds which contain glycine—NH_3CH_2COO, the smallest of the 20—have shown much promise for ferroelectric capabilities.

[Ag(NH$_3$CH$_2$COO)(NO$_3$)] was reported by Pepinsky et al. to have phase transition at 218 K [32]. It has a reported spontaneous polarization of 0.60 μC · cm^{-2} at 100 K [33]. (NH$_3$CH$_2$COO)$_2$ · MnCl$_2$ · 2H$_2$O was reported to have a spontaneous polarization of 1.3 μC · cm^{-2} at room temperature, one of the few organic ferroelectric materials to polarize at ambient conditions [34]. Some ferroelectrics have very complex phase transitions, such as betaine calcium chloride dehydrate, or [Ca[(CH$_3$)$_3$NCH$_2$COO](H$_2$O)$_2$Cl$_2$]. This MOF undergoes 8 phase transitions between its final paraelectric and ferroelectric phases, and interestingly the ferroelectric space group does not fall in the sub groups of the paraelectric space group [35]. Below 48 K, this MOF has a spontaneous polarization of 2.5 μC · cm^{-2}.

These examples of ferroelectric MOFs as well as many others are typically initially found by happenstance and are subsequently altered to discover new materials by affecting this electronic property. The goal of this work is to broadly screen MOF databases using a first principles approach to potentially discover new classes of ferroelectric and potentially multiferroic MOFs. This is accomplished by using methods covered in the next chapter.

CHAPTER 2

METHODS

In order to produce meaningful results from a search for potential ferroelectric metal-organic frameworks, several methods are implemented. In the following chapter, these methods and examples of the tools which are used to complete these tasks are described in detail. Where a specific example is deemed necessary, the MOF described by DiSante et al. [30] (henceforth called Mn-MOF) will be used as a model system.

2.1 DENSITY FUNCTIONAL THEORY

The basis of density functional theory (DFT) lies in quantum mechanics and the accuracy with which it describes the natural universe[36]. Quantum mechanical methods usually utilize electronic wavefunctions within a multibody Schrödinger equation to gain an understanding of the approximate behavior of the electrons in a given system. The major issue with determining the behavior in this way is that it scales poorly with the size of the system; each electron adds three dimensions to the equation, and in large systems the interactions between these electrons also need to be included within the Hamiltonian operator. DFT is an *ab initio* method which uses electron density instead of electronic wavefunctions to describe energy characteristics of a material. The benefit of finding the electron density as opposed to the individual wavefunctions is the density captures the overall behavior of the electrons with only three dimensions, which greatly simplifies the computation. This simplification does lead to some inaccuracy in capturing the exact behavior of the system, but in structures of the size in which this work will be exploring

(between 60 and 500 atoms), DFT is more feasible than more accurate methods while still being accurate enough to not explore more expensive methods. Many different software packages exists which utilize DFT, and this work uses the Vienna Ab-initio Simulation Package (VASP) 5.3.3 [37-40] with a projector-augmented wave (PAW) basis set and the Perdew-Burke-Ernzerhof (PBE) [41, 42] version of a generalized gradient approximation (GGA).

2.2 SCREENING PROCEDURES

One of the key goals of this project is to identify material candidates that may have ferroelectric qualities. In order to do this in an efficient manner, it is prudent to develop a means by which large numbers of structures may be sifted through quickly to remove obvious non-contenders from consideration. Although there are many qualities which several ferroelectric materials have in common, the one mutual characteristic is that the phase in which the spontaneous polarization arises is restricted to having certain symmetry operations. Of the 32 possible crystallographic point groups, only 10 of these will allow for a permanent dipole moment to exist within the structure, the polar point groups C_1, C_s, C_2, C_{2v}, C_3, C_{3v}, C_4, C_{4v}, C_6, and C_{6v} [43]. All the crystallographic point groups translate to space groups, which is the more common nomenclature for describing the symmetry of 3-dimensional structures as opposed to isolated molecules. By using material databases which list the space group, it is possible to quickly identify materials which by their structure do not have any capability of having spontaneous polarization. Mn-MOF, which we will use to describe future calculations, belongs to one of the polarizable space groups, Pna2$_1$. Within the CoRE MOF database, there are 73 MOFs

Table 1 *List of structures within the CoRE MOF database determined to belong to space group 33, as known as Pna2₁.*

ABEXEM	FIHXUR	MEJQOJ	POQXAV	VAQLAC
ABEXIQ	FOHCIP	MICCUY	RARYOZ	VASKOR
ABEXOW	FUFREE	NABCEA	RATRUB	VILXOE
ABEXUC	FULQUZ	NAKNUK	RATSAI	VIRVEY
ABEYAJ	GAJVIY	NALWOO	RATVEP	WEHJIE
ABEYEN	GURPUF	NAPZOV	RILVOZ	WIJDID
ABEYIR	HEDBOJ	NAPZUB	SODZIV	XAVDEF
AVEMOE	HEDBUP	NATXOW	TEPGUS	XAWZOM
CEHWIX	IDORIE	NEVGIE	TEQPAI	XOKHIP
CEHWOD	IJISOK	OFODAP	TOHYUL	YARFII
DAGDUL	ILAGUY	OKITAE	TOZHAR	YASLUA
DITYAH	JENKET	OLUCAZ	UBUMAH	YIZWIN
EREGOY	KEXKAB	OMAXEG	UMELUU	ZASWOF
FEFZOF	MEJQEZ	OWAVIS	UMEMAB	
FEJKEM	MEJQID	POCPAZ	UXUZAP	

that belong to this same space group and so also have the potential to be ferroelectric; these are listed in Table 1. The full screening procedure will include all 68 of the 230 total space groups in which a polar structure is possible [44].

2.3 STRUCTURE OPTIMIZATION

When a structure is selected for evaluation, it must first be fully optimized. Most databases containing structural information have the experimentally determined structure based on X-ray diffraction patterns and other spectroscopic techniques. Unfortunately, these experimental techniques occasionally will provide structures which are not physical, as shown in Figure 3. Therefore, it is often necessary to clean up and optimize the

A.   B.
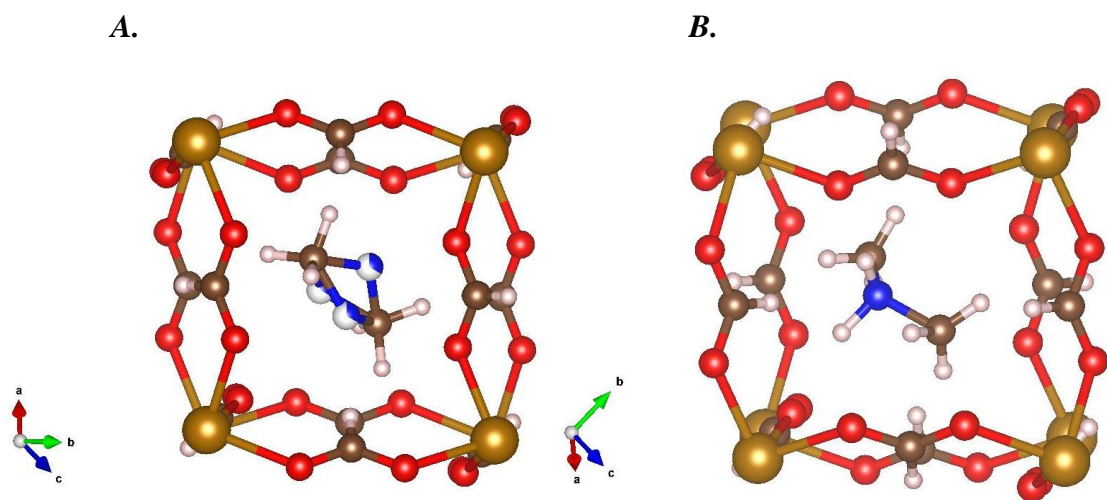
Figure 3 *Structures listed with Ref [29]. A: Structure from crystallographic techniques. B: Structure with corrected bonding geometry. The nitrogen atoms will appear equally in any of the three positions shown in A, and the phase will determine where it actually is, typical of order-disorder ferroelectric materials.*

Table 2 *Ground state energy (eV) of Mn-MOF from Ref [30] from convergence studies. The difference in energy between combinations should become closer as one moves down and right across the table, as shown. This same direction is associated with a more computationally expensive calculation.*

		K point grid		
		1x1x1	3x4x2	6x8x4
Energy cutoff (eV)	**350**	-579.91	-579.82	-579.83
	400	-579.42	-579.38	-579.42
	450	-579.15	-579.05	-579.07
	500	-579.07	-578.97	-578.99
	550	-579.14	-579.03	-579.06

structures using computational tools such as VASP. Once the structure resembles the physical system, it is important to optimize the structure to ensure that the electron density is as it should be at the ground state energy, which is the most thermodynamically stable representation possible. For Mn-MOF, the plane-wave energy cutoff for these calculations is 450 eV, and a 3x4x2 k-point grid is used, which were determined to be the ideal initial variables by convergence studies shown in Table 2. Larger values of these cutoff variables are more accurate but are also more expensive. The main purpose of the convergence studies is to better understand the ideal input variables for the calculation.

2.4 BERRY PHASE CALCULATION

Once the structure is well characterized, the next important step is to determine the dipole moments which arise in the ferroelectric phase of the material. Within VASP there is code which can compute these dipole moments using a method known as a Berry phase calculation. This version of the Berry phase calculation is derived from expressions of the "Modern theory of polarization" [45-50] and is used in the context of this work to calculate the macroscopic electronic polarization. By using the LCALPOL tag within VASP, the magnitudes of the contributions to the ionic and electronic dipole moments are determined in the directions of the lattice vectors given by the initial structure. These contributions are summed to give the magnitude and direction of the overall dipole moment which is in turn used in a simplified form of the overall polarization calculation

$$P = \frac{\Delta p}{\Delta V} \qquad\qquad 1$$

where P is the polarization and p is the dipole moment in a set volume of the given material, V. This method of determining the spontaneous polarization in Mn-MOF yields a value $P = 1.64 \ \mu C \cdot cm^{-2}$, which agrees with literature [30].

2.5 PSEUDO MODULE

Up to now only the ferroelectric phase of the material has been discussed. However, another necessary characteristic of ferroelectric materials is that the spontaneous polarization must be reversible upon reversal of an external electric field. A subtle consequence of this is that a phase transition must occur in which the structure, once polar in an arbitrary positive direction, must at some point, in order to achieve the polarization in a negative direction, have zero net dipole moment. This nonpolar pseudo-phase of the material can be thought of as a transition state between two equivalent and oppositely oriented polar structures. One important characteristic of the nonpolar structure is symmetry is added back into the material in order to contribute the net zero dipole moment. If the net zero dipole moment is achieved by reducing the individual moments to zero, the phase is termed paraelectric; if the dipole moments couple in such a way that the net dipole becomes zero without the individual dipole moments decreasing, it is termed antiferroelectric. Given the method in which the screening of these materials occurred, only the polar phase is identified in material databases. In order to confidently say that a polar structure can switch the direction of its net dipole moment in response to an external electric field, it is imperative that this high-symmetry nonpolar structure be identified. One tool which has proven itself useful for the identification of the high-symmetry phase is the PSEUDO program [51-53] located within the Bilbao
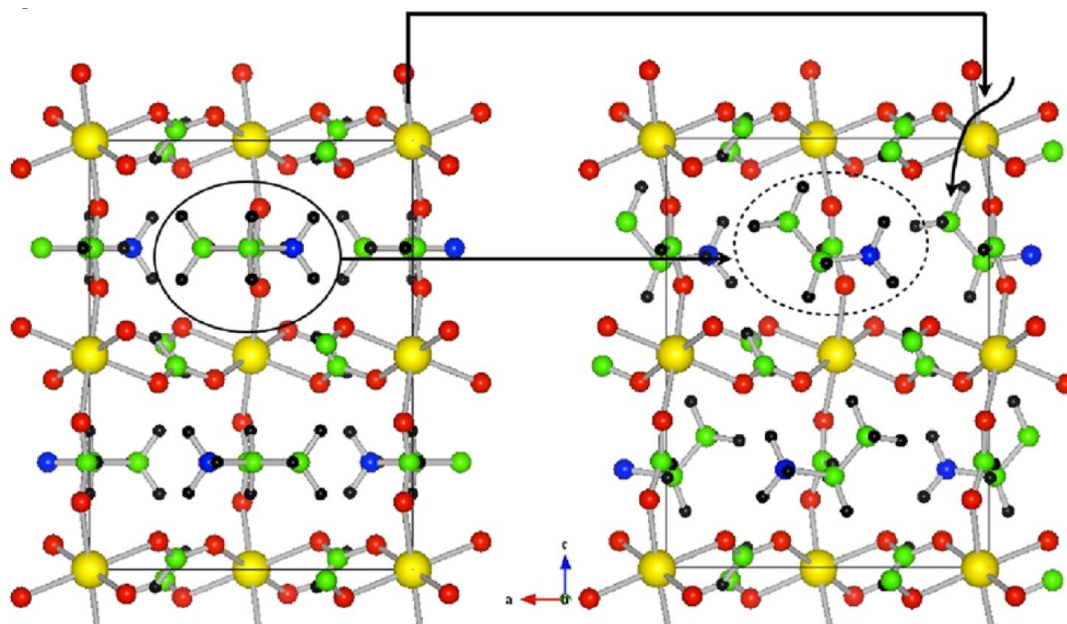
Figure 4 *Example of two phases from the structure from Ref [30]. Given the polar structure (right), the PSEUDO program can identify the distortions necessary to achieve the higher symmetry, nonpolar structure (left).*

Crystallographic Server [54-56]. If a structure, with space group X, is such that all its atomic positions x_i can be described as $x_i^o + w_i$, with w_i being small displacements, while the virtual atomic positions x_i^o have a higher symmetry described by a supergroup $Y > X$, we say that the structure is pseudosymmetric for the space group Y [57]. The objective of the PSEUDO program is to detect pseudosymmetry in a given structure and to derive a virtual parent high-symmetry structure within a user input tolerable displacement of the original structure. Figure 4 shows how Mn-MOF can switch between the two phases, of which the nonpolar one was found using this program.
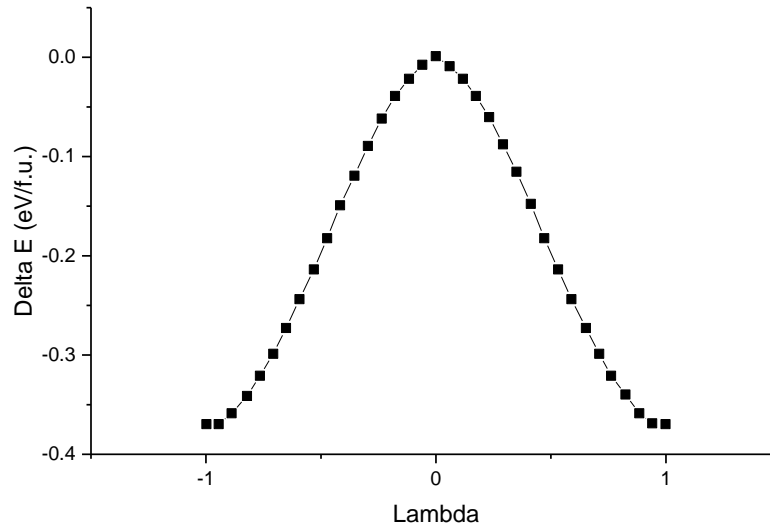
Figure 5 *Energy profile for the phase transition of Mn-MOF, adapted from Ref. [30]. Lambda values of ±1 correspond to the polar phase, while 0 is the nonpolar phase.*

2.6 NUDGED ELASTIC BAND METHOD

Unfortunately, identifying the polar and nonpolar phases of a material does not by itself constitute ferroelectricity. There must exist a continuous, physical pathway between these two phases in order for the ferroelectric condition to be met fully. One convenient way to do this which is already implemented within VASP is the nudged elastic band (NEB) method [58, 59]. The NEB method's primary function is to calculate the minimum energy pathway (MEP) between a well-defined initial and final state. The MEP is typically initialized by creating images which form a linear interpolation between these initial and final structures; the method then minimizes the energy of this sequence of images. Once the energy is minimized, these images represent the true MEP between the

initial and final states [60]. A variation on NEB, known as climbing image NEB (cNEB), is typically used to calculate the energy barrier between two known states by forcing one of the regular NEB images to sit at the transition state along the MEP [61]. This is especially useful when characterizing a reaction pathway. In the context of this work, the initial and final states would correspond the polar structures which orient up and down, respectively, and the transition state would be the nonpolar structure. While the energy barrier may provide some hint as to the plausibility of the spontaneous polarization reversing, its magnitude is not relevant for this work. Rather, the aim is to show that a continuous, physical pathway exists from one polar structure, to the nonpolar structure, and eventually to the opposite-facing polar structure. An example of this continuous phase transition is shown for Mn-MOF in Figure 5.

2.7 CONCLUSIONS

By using first principles calculations, it has been shown that it is possible to capture typical ferroelectric behavior in MOFs. The combination of Berry phase calculations and cNEB method within VASP, along with PSEUDO from the Bilbao Crystallographic Server, are used to effectively identify candidates for ferroelectricity. The next step is to apply this formalism to MOF databases to determine previously unknown but potentially useful molecular electronic materials.

CHAPTER 3

RESULTS

Using all the methods from the previous chapter, it is possible to identify a structure as ferroelectric, and further analysis can be done to determine multiferroicity. However, applying this methodology to individual structures is only satisfying on a small scale. The more meaningful approach would be to utilize these methods for screening hundreds of materials to potentially discover dozens of viable materials for various ferroelectric applications. Figure 6 shows one such algorithm for doing this large-scale screening. As a first pass to reduce the number of total calculations which are done, the algorithm is restricted to the CoRE MOF database, which is a subset of the Cambridge Structural Database and contains only those MOFs which are experimentally-realized, computationally-ready, three-dimensional, and porous, approximately 5000 in total [21]. From here, the database is screened further for materials which have a nonzero dipole moment associated with the structure. These structures are then further explored to determine the potential for a phase transition into a nonpolar, centrosymmetric phase. If one exists, the path of this phase transition is quantified using Berry phase calculations and NEB as described in the previous chapter. In an effort to validate this algorithm, it is first implemented on a smaller group.

3.1 SCREENING OF SPACE GROUP PNA2$_1$

Throughout Chapter 2, Mn-MOF [30] was used to explain the methods of determining ferroelectricity in molecular materials. The ferroelectric phase of this MOF is known to belong to space group 33, or Pna2$_1$. As described in Table 1, there are 73 other MOFs
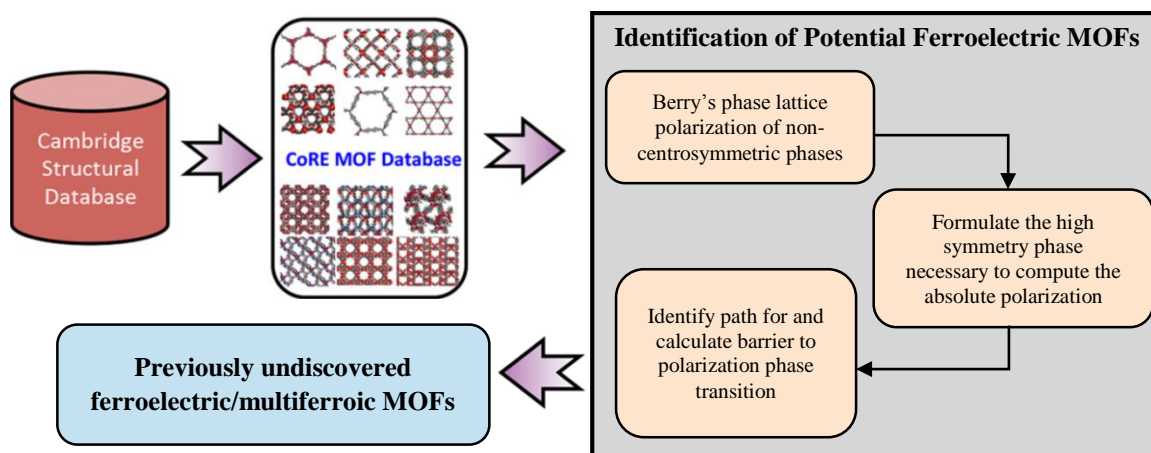
Figure 6 *Schematic illustration of the screening algorithm for identification of new ferroelectric MOFs. Berry phase calculation will be used in initial polarization determination, PSEUDO module from the Bilbao Crystallographic Server can find high-symmetry phases, and nudged elastic band method will assist in identifying how the polarization switches.*

which also exhibit this symmetry. As a starting point for testing the screening algorithm, these 73 structures are a useful initial group given the understanding of how a ferroelectric phase transition could happen from this polar phase.

3.1.1 Polarization values

To determine which of the MOFs from the Pna2$_1$ space group has potential to be explored as a worthwhile ferroelectric material, the magnitude of the spontaneous polarization in each is calculated. Using the Berry phase method within VASP, the dipole moment of each material's unit cell is determined. From this the total spontaneous polarization is computed via Eqn. 1 and reported in Figure 7. One of the complications of calculating the polarization of a material is evident by this figure given that most of these values of polarization are higher than the best inorganic ferroelectric materials; the
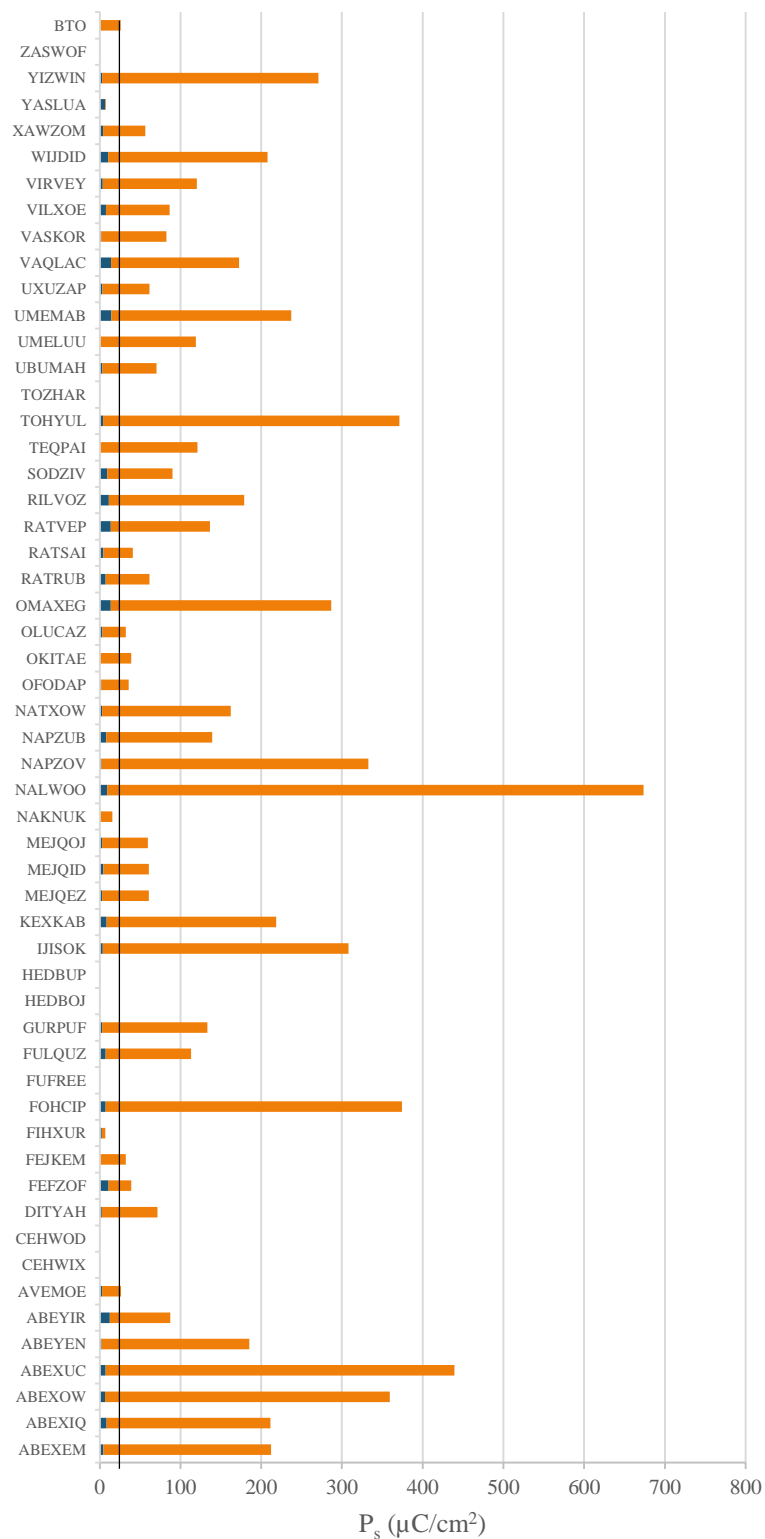
Figure 7 *Total spontaneous polarization on the 54 of the 73 structures of the Pna2₁ space group within the CoRE MOF database for which the calculation completed. The blue bars represent the electronic contribution to this polarization. The black line represents the value of Pₛ for BaTiO₃ (BTO).*
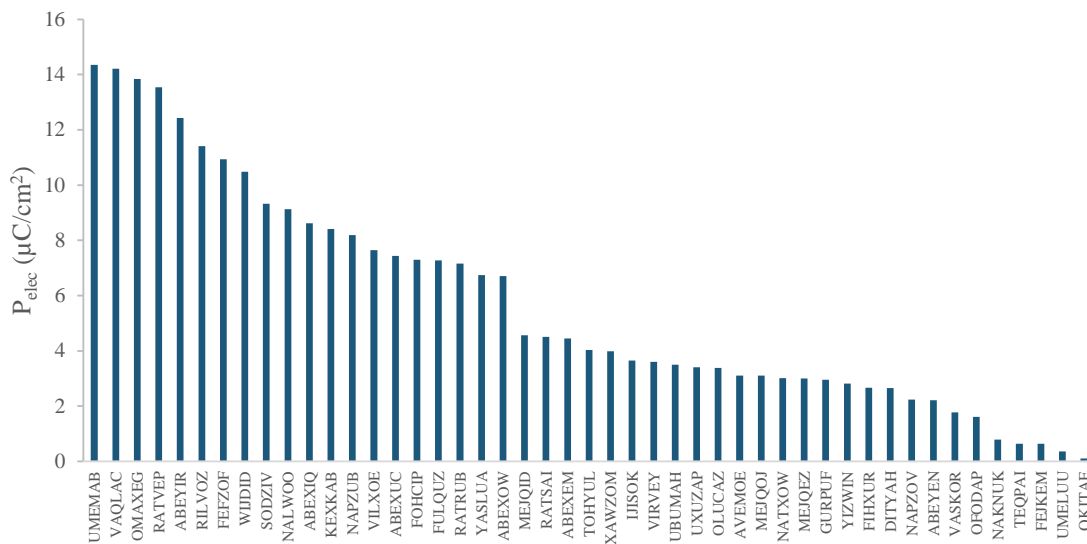
Figure 8 *Spontaneous polarization as calculated from the electronic contribution to the dipole moment of the CoRE MOFs from the Pna2₁ space group.*

spontaneous polarization of $BiTiO_3$ (BTO), a common inorganic ferroelectric, is shown in Figure 7 as a reference point at 26 $\mu C \cdot cm^{-2}$. The artifact which causes this phenomena is known as the quanta of polarization [62]. The calculation of the ionic (or that of the nucleus plus the core electrons) contribution to the dipole moment of a periodic structure can change dramatically based on the point of reference, unlike the dipole moment of an isolated molecule which is deterministic [63]. This artifact is the reason why the nonpolar centrosymmetric phase of the material must be found to determine the spontaneous polarization; different phases of the same material will have the same artifact, so the difference in polarization between the two phases can be reported as the true spontaneous polarization. The electronic (or that of the valence electrons) contribution to the dipole moment is not susceptible to this same issue, so the value of polarization based solely on
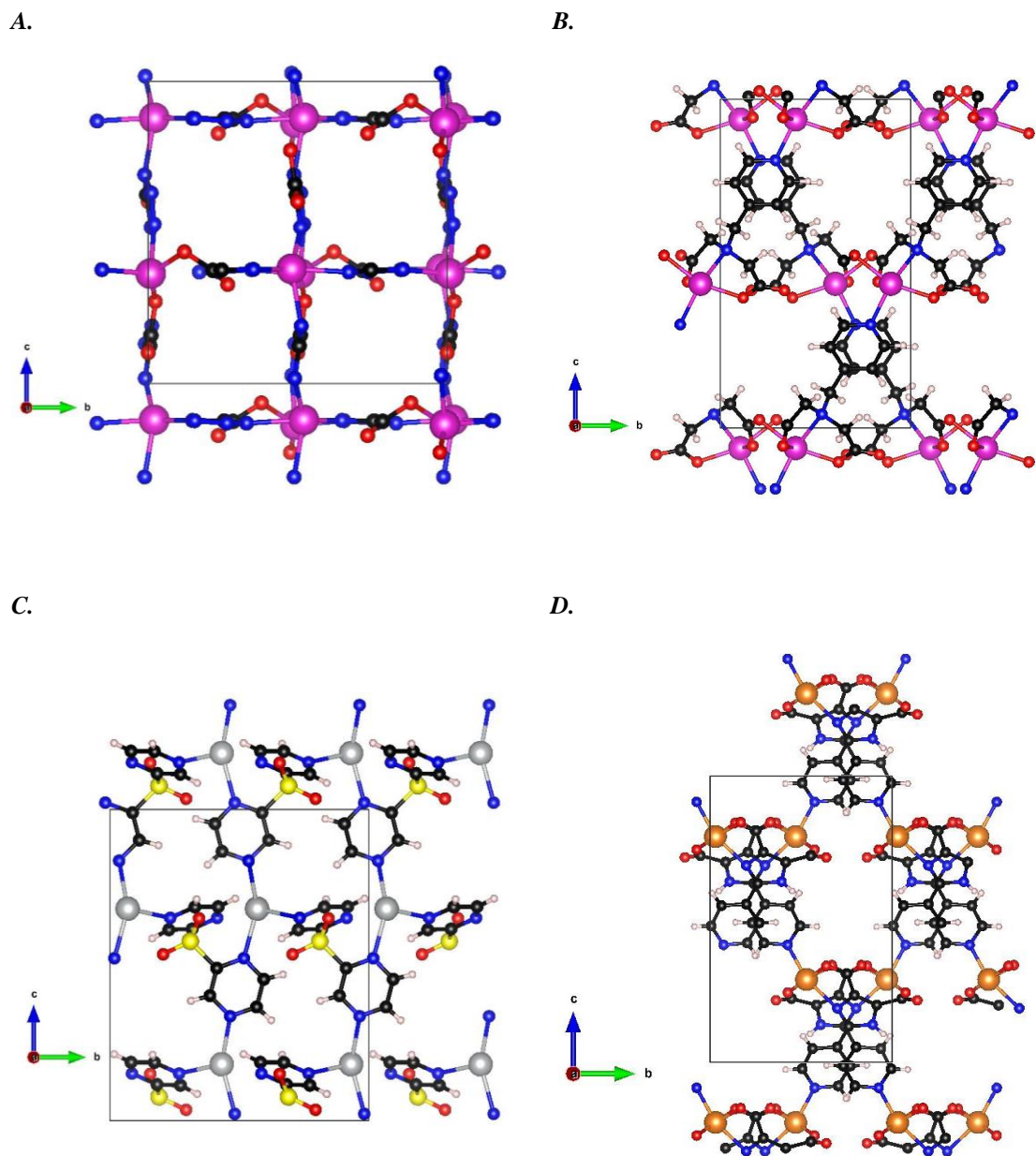
Figure 9 *Visualizations of the structures with the four highest P_{elec} values from the Pna2$_1$ space group. Atom colors are as follows: Pink, Cd; Grey, Ag; Orange, Mg; Black, C; Blue, N; Red, O; Ivory, H; Yellow, S. The structure names are as follows: **A.** UMEMAB, **B.** VAQLAC, **C.** OMAXEG, **D.** RATVEP.*

Table 3 The structures belonging to the Pna2$_1$ space group from the CoRE MOF database which included a known ferromagnetic metal node. Only those structures for which a spontaneous polarization value was able to be determined are included.

Structure	Metal Node	P$_{elec}$	P$_s$
RILVOZ	Mn	11.41	167.39
FEFZOF	Co, Hg	10.93	28.21
WIJDID	Cu	10.48	197.48
VILXOE	Mn	7.64	78.97
YASLUA	Hg, Mn	6.74	1.09
OLUCAZ	Cu	3.38	29.02
YIZWIN	Cd, Ni	2.81	267.92
DITYAH	Co	2.66	68.95
FEJKEM	Hg, Mn	0.64	31.61

this contribution can better determine which material can be interesting to investigate more thoroughly. This incomplete value of polarization is reported for the Pna2$_1$ structures in Figure 8, and the top four promising candidates for ferroelectricity from this figure are shown in Figure 9 to demonstrate the wide variety of complexes which can give rise to these phenomena.

3.1.2 Potential for ferromagnetism

One of the goals of this project is to look into the possibility of multiferroic molecular materials. One pragmatic way to do this is to identify those ferroelectric MOFs which already have metal centers known for carrying ferromagnetic properties. While this does not ensure that the MOF will be multiferroic, several studies have shown that a ferromagnetic bulk metal will often retain that property in a hybrid system [64-73]. Those MOFs from the Pna2$_1$ space group which displayed a polarization and have a metal center with known ferromagnetic qualities are listed in Table 3.

3.2 SCREENING ALL POLAR SPACE GROUPS

The previous section focused solely on one space group which by symmetry allows for the potential for ferroelectric phases of materials. This space group is not the only one which has the proper combination of symmetry operations to allow for ferroelectric compounds. The following sections explore these other possibilities.

3.2.1 Converting point groups to space groups

As mentioned before, only 10 of the 32 crystallographic point groups will allow for a permanent dipole moment to exist within the structure: C_1, C_s, C_2, C_{2v}, C_3, C_{3v}, C_4, C_{4v}, C_6, and C_{6v}. An important feature of all these point groups is that more than one point remains unmoved; this is a requirement of polar point groups. If a point group contains a mirror plane perpendicular to a rotation axis or more than one rotation axis, it cannot be polar. While point groups are handy for identifying the symmetry in molecules, crystals can have many more subtle symmetry elements not contained in the simple point group definitions. Therefore it is necessary to specify further identifiers for 3-dimensional crystals; these are called space groups. There exists a total of 230 space groups which are derived from the crystallographic point groups. Table 4 shows how these space groups correlate to each of the polar point groups, and also which of the seven crystals systems they belong to. Of the 230 space groups, 68 of them contain symmetries which allow for the potential a dipole moment, and by extension polarizability. Within the CoRE MOF database, there are 668 structures which are labelled as being a member of these polar space groups. With the exception of those belonging to the triclinic P1 space group, the polarization of all of these structures was determined through the same methods listed above and are reported in the next section.

Table 4 *List of the polar space groups and to which crystal systems and crystallographic point groups they belong. Also listed are the number of structures labelled as belonging to these space groups according to the CoRE MOF database.*

Crystal system	Point group	Space group	Structures
Triclinic	C_1	P1	122
Monoclinic	C_2	P2	4
		$P2_1$	68
		C2	36
	C_s	Pm	2
		Pc	17
		Cm	4
		Cc	79
Orthorhombic	C_{2v}	Pmm2	0
		$Pmc2_1$	1
		Pcc2	0
		Pma2	0
		$Pca2_1$	14
		Pnc2	5
		$Pmn2_1$	3
		Pba2	1
		$Pna2_1$	73
		Pnn2	6
		Cmm2	0
		$Cmc2_1$	15
		Ccc2	0
		Amm2	2
		Abm2	0
		Ama2	3
		Aba2	3
		Fmm2	1
		Fdd2	29
		Imm2	5
		Iba2	11
		Ima2	4
Tetragonal	C_4	P4	2
		$P4_1$	11
		$P4_2$	0

Table 4 (continued)

Crystal system	Point group	Space group	Structures
Tetragonal	C_4	$P4_3$	20
		I4	4
		$I4_1$	5
	C_{4v}	P4mm	0
		P4bm	0
		$P4_2$cm	0
		$P4_2$nm	0
		P4cc	1
		P4nc	3
		$P4_2$mc	0
		$P4_2$bc	3
		I4mm	0
		I4cm	1
		$I4_1$md	5
		$I4_1$cd	9
Trigonal	C_3	P3	2
		$P3_1$	3
		$P3_2$	5
		R3	14
	C_{3v}	P3m1	0
		P31m	0
		P3c1	2
		P31c	7
		R3m	3
		R3c	16
Hexagonal	C_6	P6	0
		$P6_1$	27
		$P6_5$	5
		$P6_2$	2
		$P6_4$	0
		$P6_3$	4
	C_{6v}	P6mm	0
		P6cc	1
		$P6_3$cm	4
		$P6_3$mc	1

3.2.2 Polarization values

The following pages show the values of the contribution to the polarization from the electronic dipole moment. This data is primarily organized by crystal class. When possible, the visualizations of the top candidates from each crystal system is shown with the largest contribution to the dipole moment pointing upwards. For the results of the calculation of the total spontaneous polarization, see Appendix I.

3.2.2.1 Monoclinic structures
The CoRE MOF database lists 210 structures which are in a monoclinic polar space group. A Berry phase calculation was done to each of these structures to determine which may be interesting to study further. Of these, 96 of the calculations converged to a viable solution, and 65 of these resulted in a nonzero value of dipole moment. The contribution of the electronic dipole moment to the polarization of these structures can be found in Figure 10 and Figure 12, and visual representations of the top performing MOFs are shown in Figure 11 and Figure 13. The $P2_1$ space group is split from the others solely for clarity in representation of the polarization plot.

3.2.2.2 Orthorhombic structures
Of the 176 structures listed in the CoRE MOF database as belonging to an orthorhombic polar space group, 73 belong to the $Pna2_1$ space group previously discussed. From the 103 structures which remained, 53 Berry phase calculations converged and 40 structures were found to have a dipole moment. These values of electronic polarization are shown in Figure 14, and the 3 structures which showed the largest electronic contribution to the polarization are represented in Figure 15. These three are especially intriguing because the value of polarization is significantly larger than BTO, which is held as the standard for inorganic ferroelectrics.

Figure 10 *Structures of the monoclinic space groups with the exception of P2$_1$ which were determined to have a dipole moment. Polarization is calculated using only the electronic contribution to the dipole moment.*

Figure 11 *Visualizations of the structure with the two highest P$_{elec}$ values from the monoclinic space groups, without P2$_1$. Atom colors are as follows: Grey, Zn; Pale blue, Cu; Black, C; Blue, N; Red, O; Ivory, H. The structure names are as follows: **A.** LAZJAZ, **B.** BAHGUN04.*

Figure 12 *Structures of the monoclinic space group P2₁ which were determined to have a dipole moment. Polarization is calculated using only the electronic contribution to the dipole moment.*

Figure 13 *Visualizations of the structure with the two highest P_{elec} values from the monoclinic space group P2₁. Atom colors are as follows: Grey, Zn; Black, C; Blue, N; Red, O; Ivory, H; Yellow, F. The structure names are as follows: **A.** FIPWUY, **B.** PAMHES.*
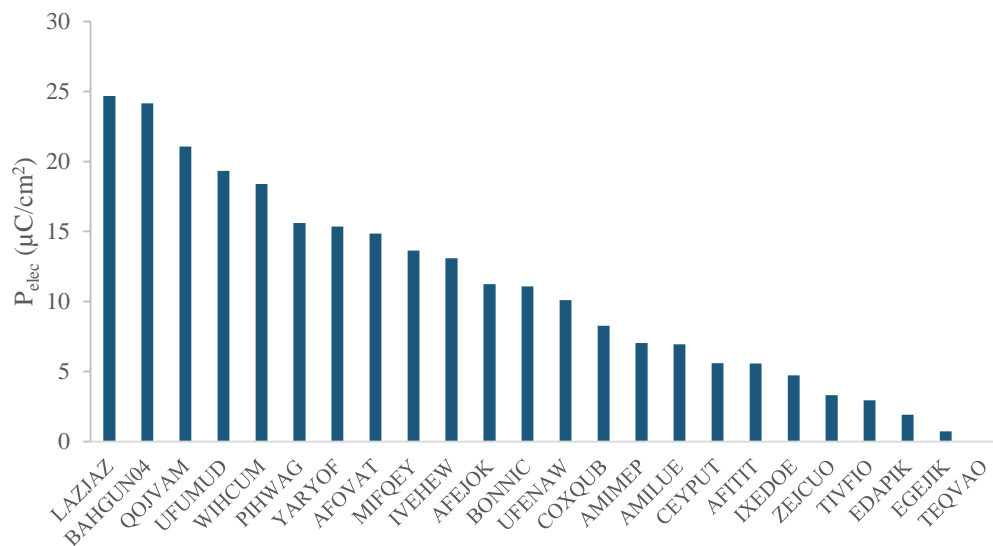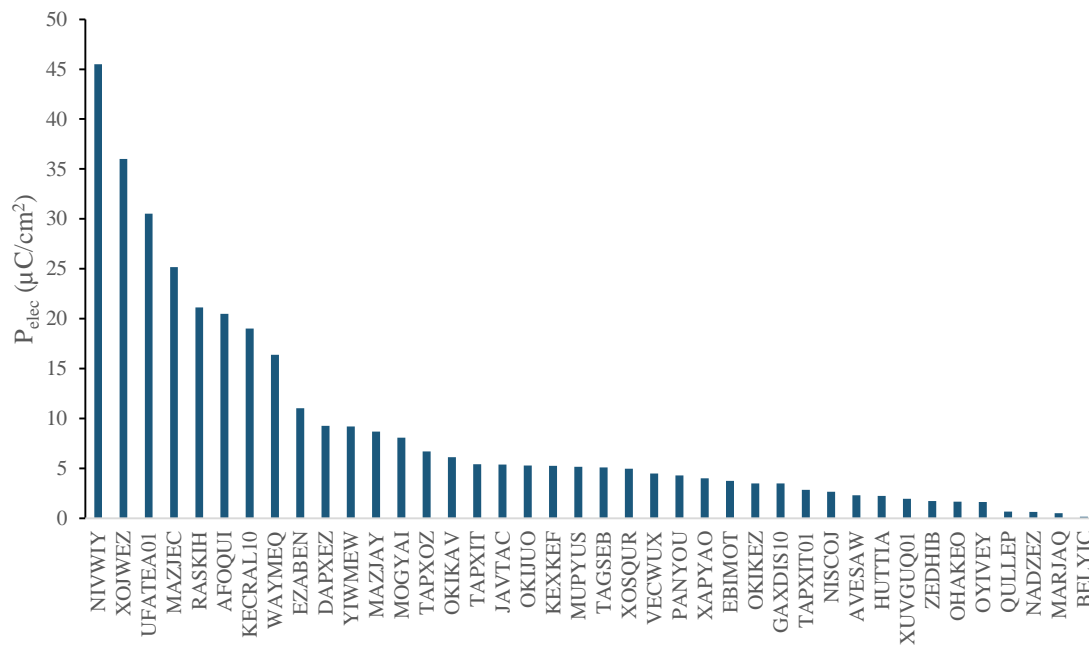
Figure 14 *Structures of the orthorhombic space groups with the exception of Pna2₁ which were determined to have a dipole moment. Polarization is calculated using only the electronic contribution to the dipole moment.*
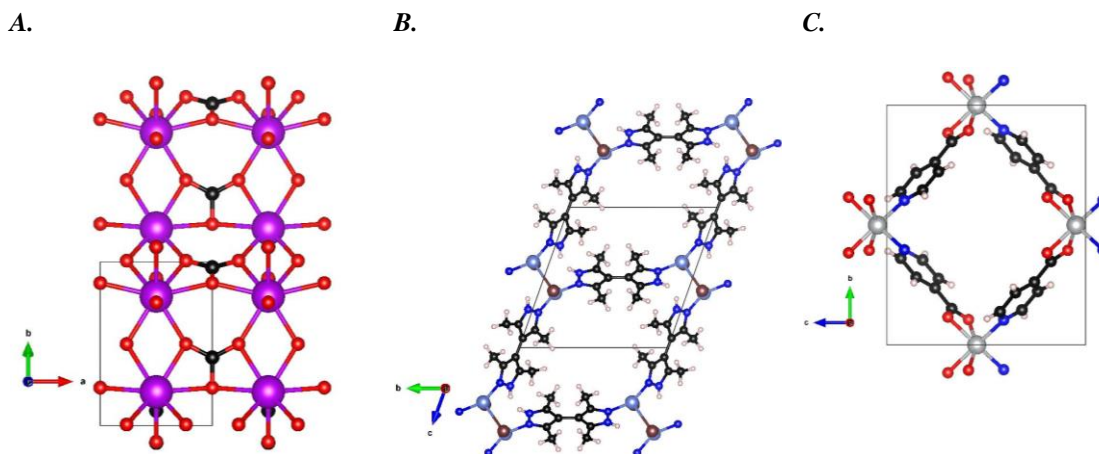
Figure 15 *Visualizations of the structure with the three highest P$_{elec}$ values from the orthorhombic space groups. Atom colors are as follows: Magenta, Gd; Pale blue, Cu; Grey, Ni; Black, C; Blue, N; Red, O; Ivory, H; Brown, Br. The structure names are as follows: **A.** NIVWIY, **B.** XOJWEZ, **C.** UFATEA01.*
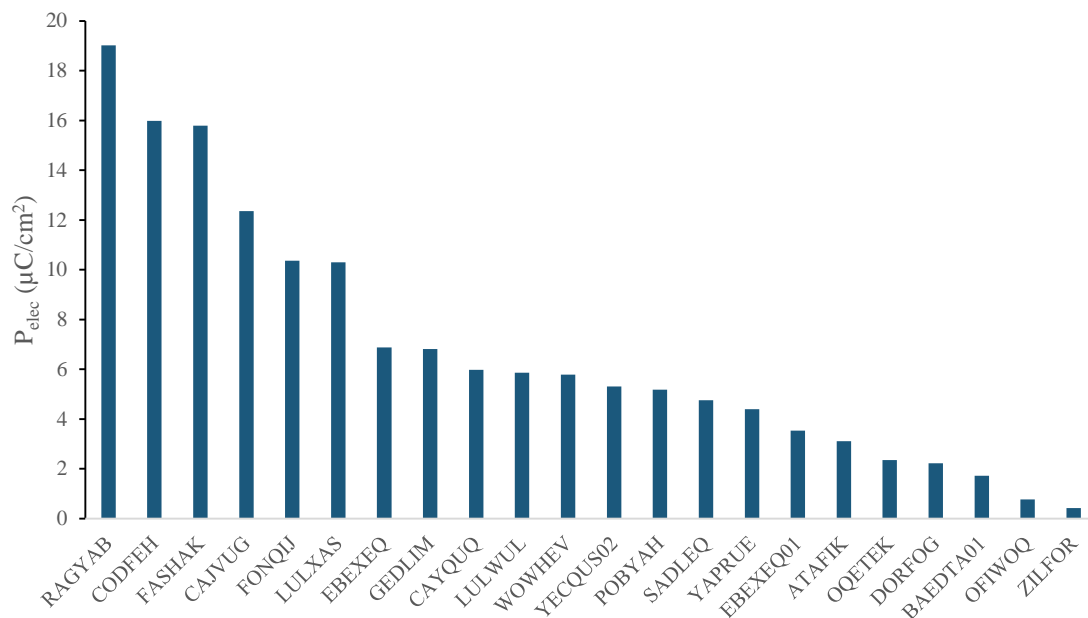
Figure 16 *Structures of the tetragonal space groups which were determined to have a dipole moment. Polarization is calculated using only the electronic contribution to the dipole moment.*

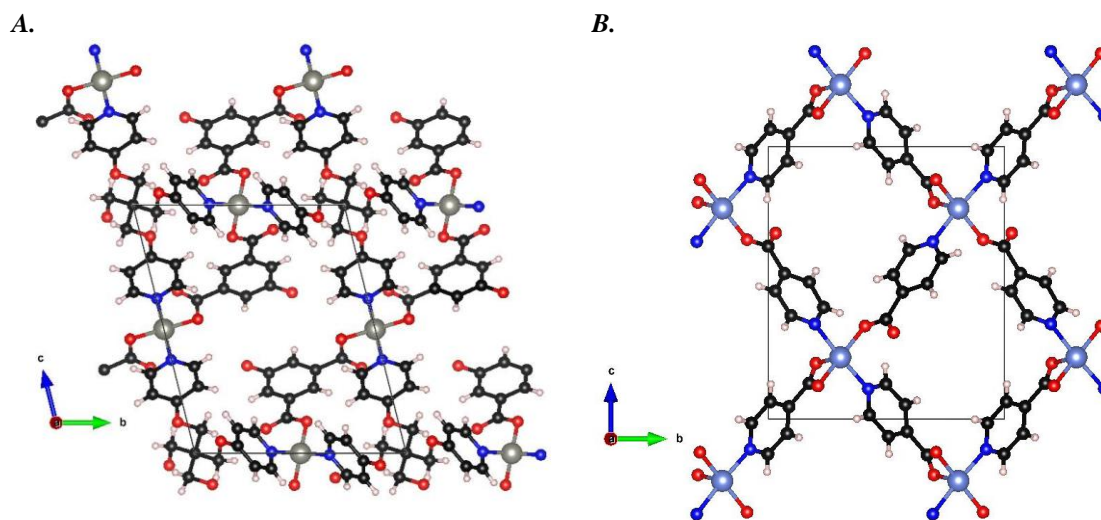**Figure 17** *Visualizations of the structure with the two highest P_{elec} values from the tetragonal space groups. Atom colors are as follows: Green, Ba; Magenta, Mn; Purple, Ge; Black, C; Red, O; Ivory, H. The structure names are as follows: **A.** RAGYAB, **B.** CODFEH.*
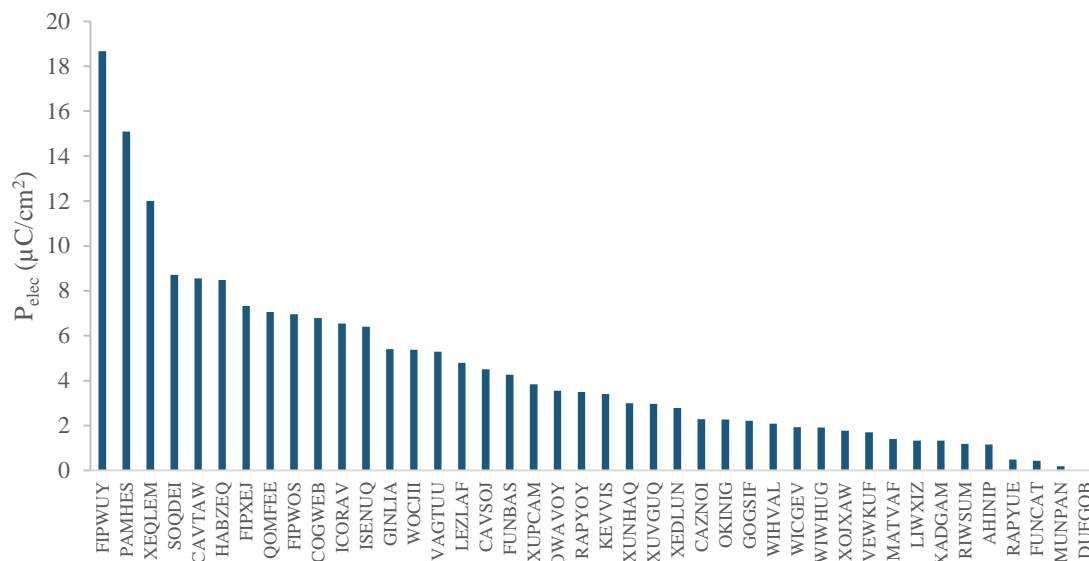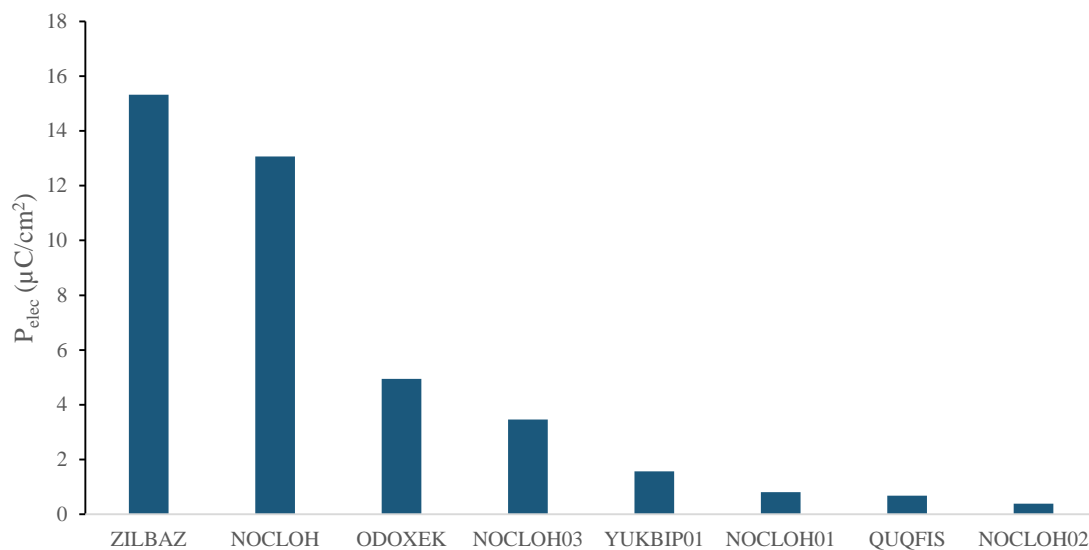
Figure 18 *Structures of the trigonal space groups which were determined to have a dipole moment. Polarization is calculated using only the electronic contribution to the dipole moment.*
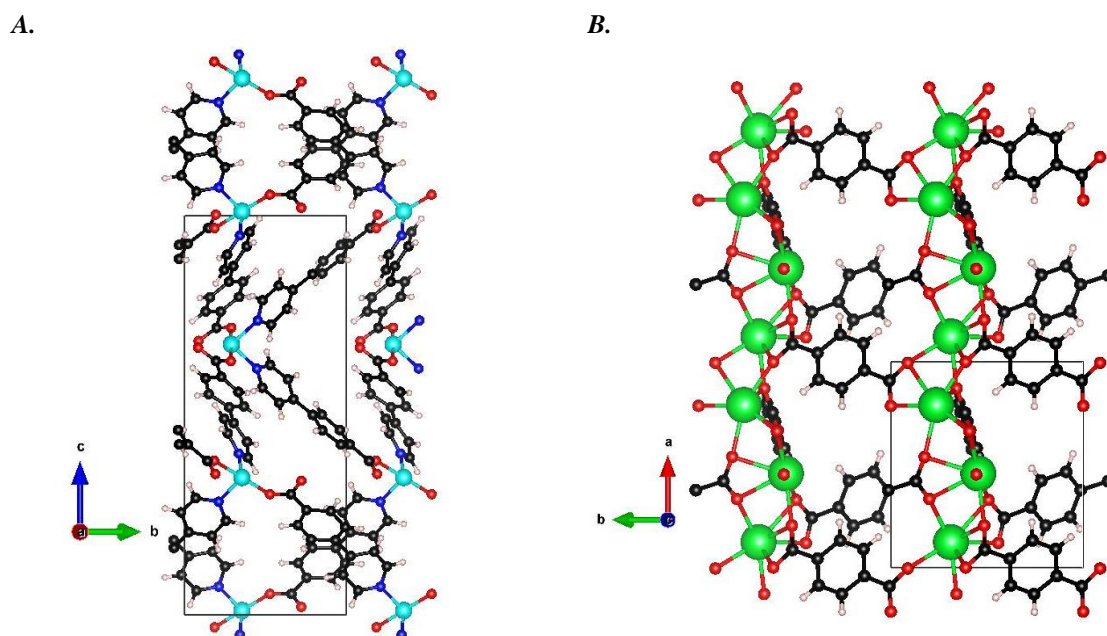
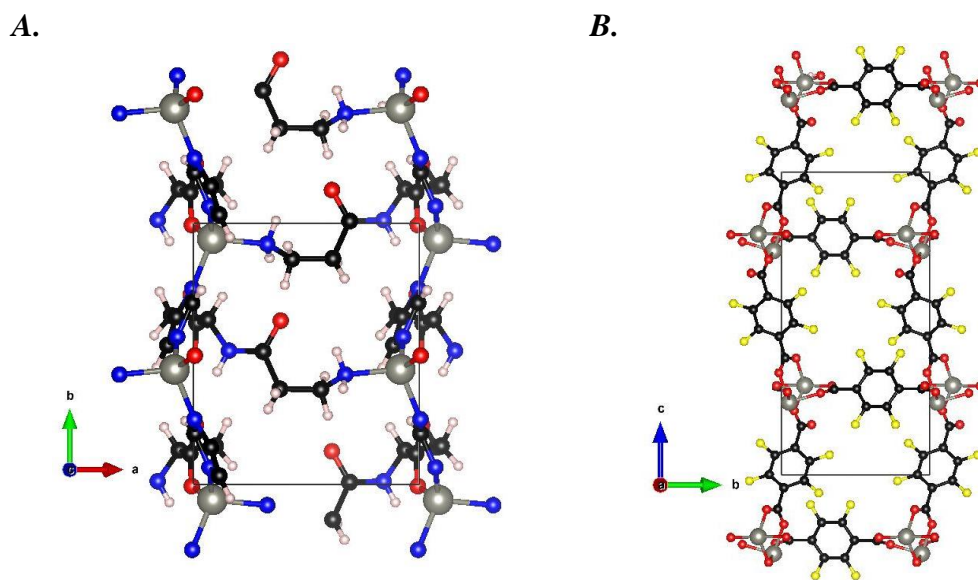**Figure 19** *Visualizations of the structure with the two highest P$_{elec}$ values from the trigonal space groups. Atom colors are as follows: Teal, Co; Green, Sr; Purple, Ge; Black, C; Blue, N; Red, O; Ivory, H. The structure names are as follows: **A.** ZILBAZ, **B.** NOCLOH.*
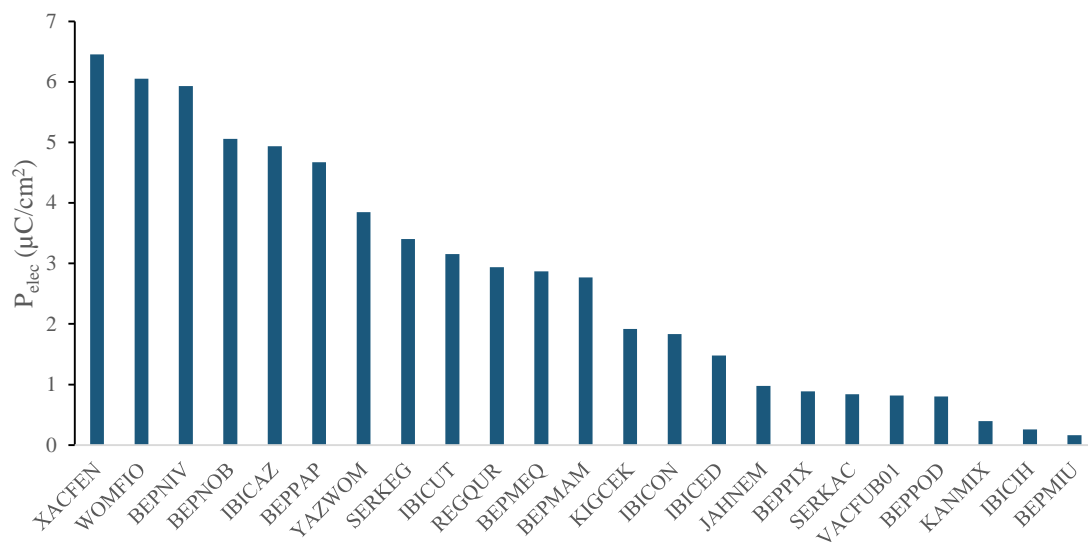
Figure 20 *Structures of the hexagonal space groups which were determined to have a dipole moment. Polarization is calculated using only the electronic contribution to the dipole moment.*
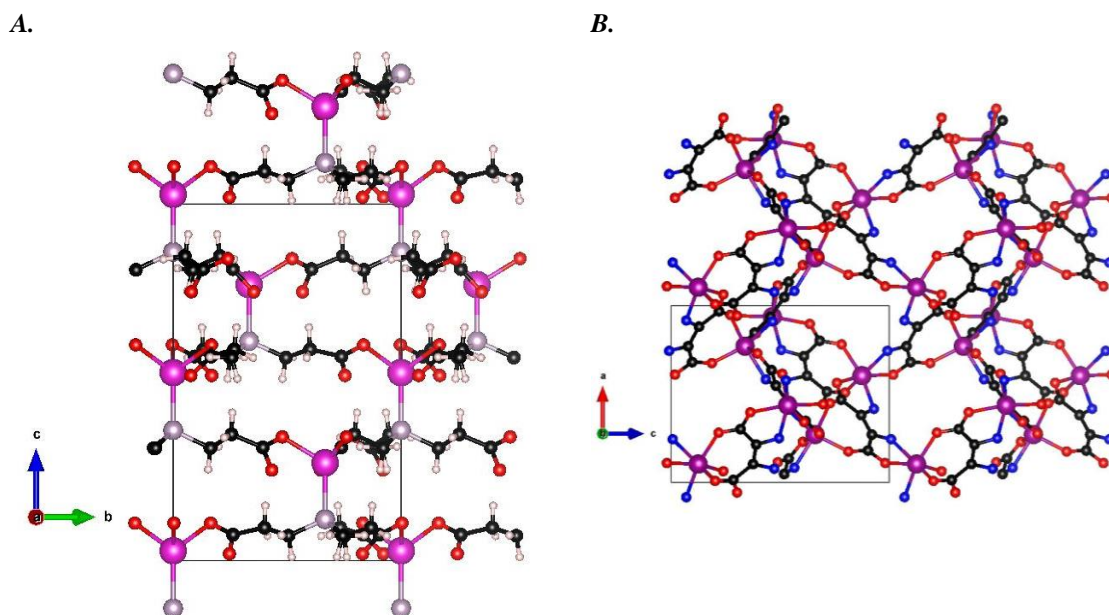
Figure 21 *Visualizations of the structure with the two highest P_{elec} values from the hexagonal space groups. Atom colors are as follows: Pink, Cd; Purple, Mn; Grey, P; Black, C; Blue, N; Red, O; Ivory, H. The structure names are as follows: **A.** XACFEN, **B.** WOMFIO.*
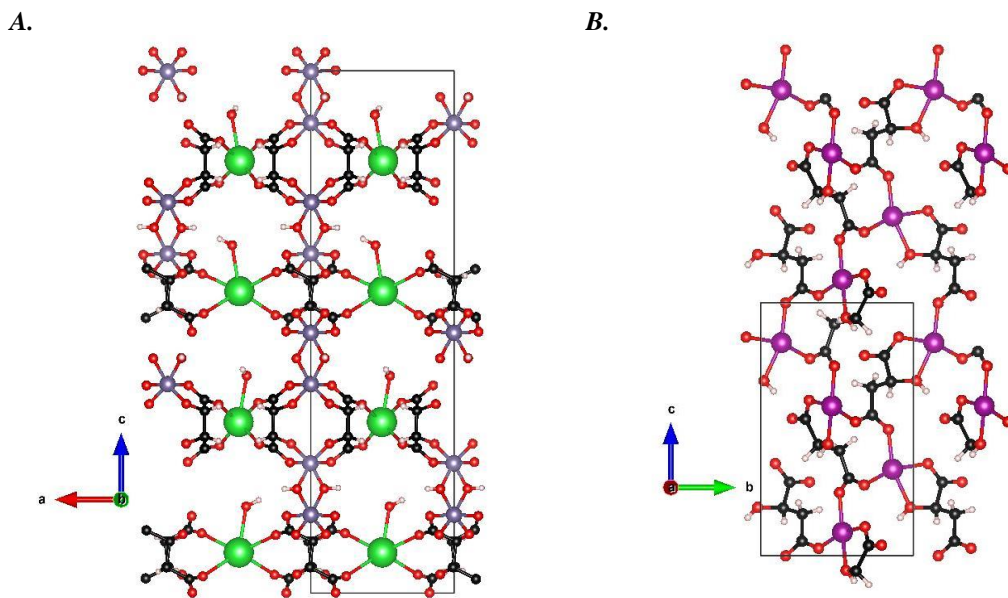
3.2.2.3   Tetragonal structures
There are 64 structures reported which belong to a tetragonal polar space group, and of the 32 in which the calculation converged, 22 recorded a dipole moment. The value of polarization based on these dipole moments is plotted in Figure 16, and two high performing structures from this crystal system are shown in Figure 17.

3.2.2.4   Trigonal structures
Of the 52 structures belonging to trigonal polar space groups, 12 of the Berry phase calculations converged resulting dipole moments in 8 structures. Figure 18 shows the electronic contribution to the polarization. Two high performing structures are shown in Figure 19.

3.2.2.5   Hexagonal structures
Hexagonal polar space groups in the CoRE MOF database contain 44 structures, of which 27 calculations converged and 23 had a dipole moment. The polarization of these structures is shown in Figure 20. The two highest performing structures are shown in Figure 21, but even these highest polarization values of this crystal system do not compare to the current performance of applied ferroelectric materials.

3.2.2.6   Triclinic structures
The triclinic polar space group P1 contains 124 structures in the CoRE MOF database. These structures were not explored in the scope of this thesis, but given that the symmetries of this group only include the identity operator, it is thought that most of these structures include some level of disorder which would disallow ferroelectric switching.

3.2.3   High potential candidates

Over the course of this project, 546 structures were tested for potential ferroelectric properties. From the 205 structures which showed a dipole moment, several materials appear to have large enough magnitudes of polarization to be used in current ferroelectric applications. Three in particular seem to have values of spontaneous polarization which surpass current inorganic ferroelectrics. The structures known as NIVWIY [74], XOJWEZ [75], and UFATEA01 [76] demonstrated an electronic contribution to polarization at values of 45.50 $\mu C \cdot cm^{-2}$, 35.99 $\mu C \cdot cm^{-2}$, and 30.53 $\mu C \cdot cm^{-2}$, respectively, which is substantially higher than the 26 $\mu C \cdot cm^{-2}$ reported in BTO. XOJWEZ has already been shown to have ferroelectric activity, but has only been investigated for a small range of temperatures [75]. More investigation would be needed to definitively claim that these other materials are indeed ferroelectric, but identifying the magnitude of potential polarization is an important first step.

3.3   FUTURE DIRECTIONS

Once the initial screening of potential ferroelectric MOFs is complete, the next step in furthering this research could be in any one of several different directions. Applications which require a higher value of spontaneous polarization could use previously discovered ferroelectric MOFs as the starting point in developing new desirable MOFs. Multiferroicity can be achieved in a ferroelectric material by including elements or molecules which naturally have magnetic moments, whether by replacement or addition in a MOF cavity. These options are explored in subsequent sections.
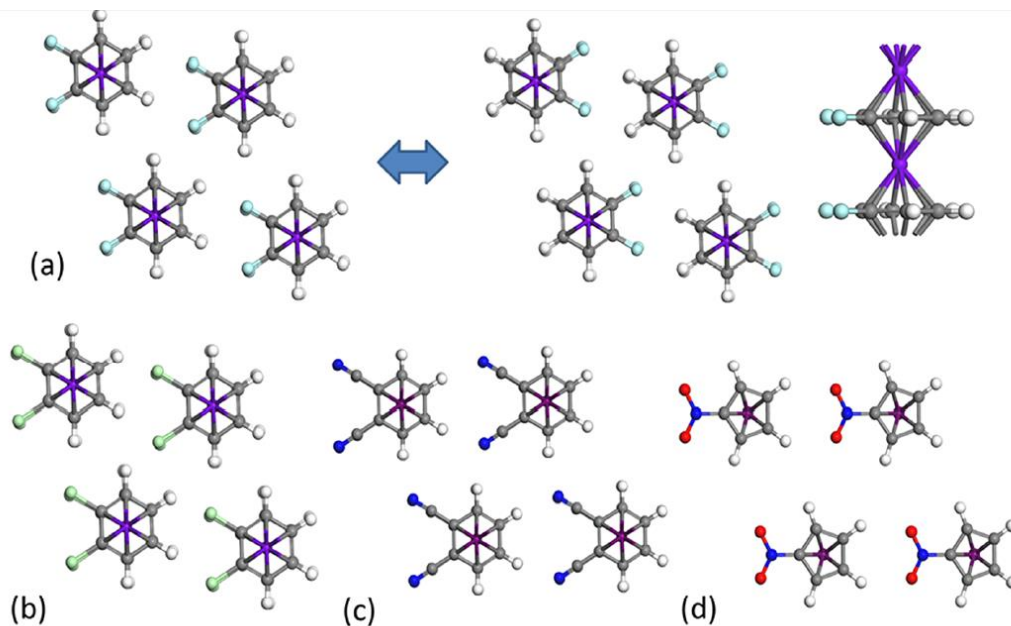
Figure 22 *Examples of SNW from Ref [77]. Vanadium is sandwiched between benzene or cyclopentadienyl with two neighboring hydrogens substituted with various species:* (a) –F, (b) –Cl, (c) –CN, and (d) –NO$_2$. *Atom colors are as follows: Purple, V; Grey, C; White, H; Red, O; Blue, N; Pale blue, F; Green, Cl.*

3.3.1 From ferroelectric to multiferroic

In a previous section, ferroelectricity was found to exist in [(CH$_3$)$_2$NH$_2$]Zn(HCOO)$_3$ [28].

Also discussed in the same publication is the potential for changing the metal center to

tailor the material for a particular application. By exchanging the zinc with a transition

metal ion—such as Mn, Fe, Co, or Ni—weak ferromagnetic ordering is realized in the

material while retaining the ferroelectric properties of the parent structure [29]. It is

reasonable to assume the same could be done with other ferroelectric MOFs with non-

ferromagnetic metal centers as long as the coordination of these metal nodes does not

change between related structures. Another way to introduce ferromagnetism to a

35
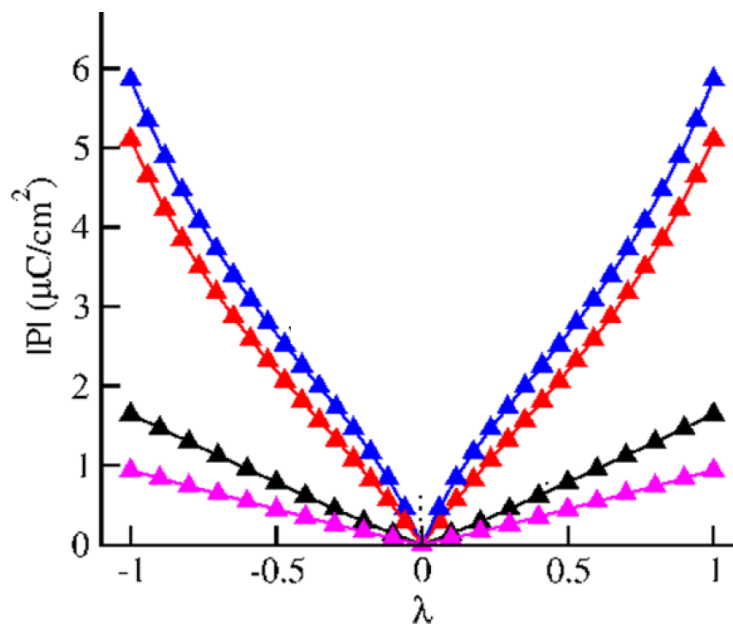
Figure 23 *Polarization curves resulting from tuning of A-groups from Ref [30]. The original organic molecule, $[CH_3CH_2NH_3]^+$ (black), has atoms replaced to capture the behavior of different systems. The other molecules include $[CH_3CH_2PH_3]^+$ (pink), $[CF_3CH_2NH_3]^+$ (red), and $[CF_3CH_2PH_3]^+$ (blue).*

ferroelectric material is described by Wu et al [77]. In the sandwich nanowires (SNW) described there and shown in Figure 22, metal ions and polar, cyclic organic molecules—such as substituted benzene and cyclopentadienyl—are stacked in such a way that a dipole moment exists along the wire which can be switched by an external electric field. In some of the example SNWs, the metal ions have an existing ferromagnetic moment. It is reported that changing the organic molecule can have an effect on the magnetic moment of the overall structure, either increasing or decreasing to the point of eliminating the magnetic moment. This phenomena was realized by replacing the substituted benzene and cyclopentadienyl molecules with croconic acid. It can be

assumed that a similar effect would occur in other metal-organic systems, such as the

MOFs detailed throughout this work, although little work has been done to verify this.

3.3.2   Engineering higher polarization in MOFs

Other applications for ferroelectric MOFs may require a specific value of spontaneous

polarization in the material. In the several instances in the literature in which tuning the

polarization of a hybrid material is desired, this is achieved primarily through exchanging

the organic portion of the material. The SNWs from the previous section would have

different functional groups substituted for neighboring hydrogen atoms on the benzene or

cyclopentadienyl rings [77], as shown in Figure 22. Di Sante et al. showed that the

polarization of $[CH_3CH_2NH_3]Mn(HCOO)_3$ can be tuned by substitution of particular

atoms on the ethylammonium molecule [30], as shown in Figure 23. Given the wide

variety of organic molecules with inherent dipole moments, a large number of materials

with a tuned polarization could be derived from any ferroelectric or multiferroic MOF of

interest.

APPENDIX I

This section shows the values of the total spontaneous polarization as the calculation was described in Chapter 2 for all of the structures discussed in this work for which the calculation produced a dipole moment. The figures are organized by crystal system, similarly to how they were in Chapter 3.
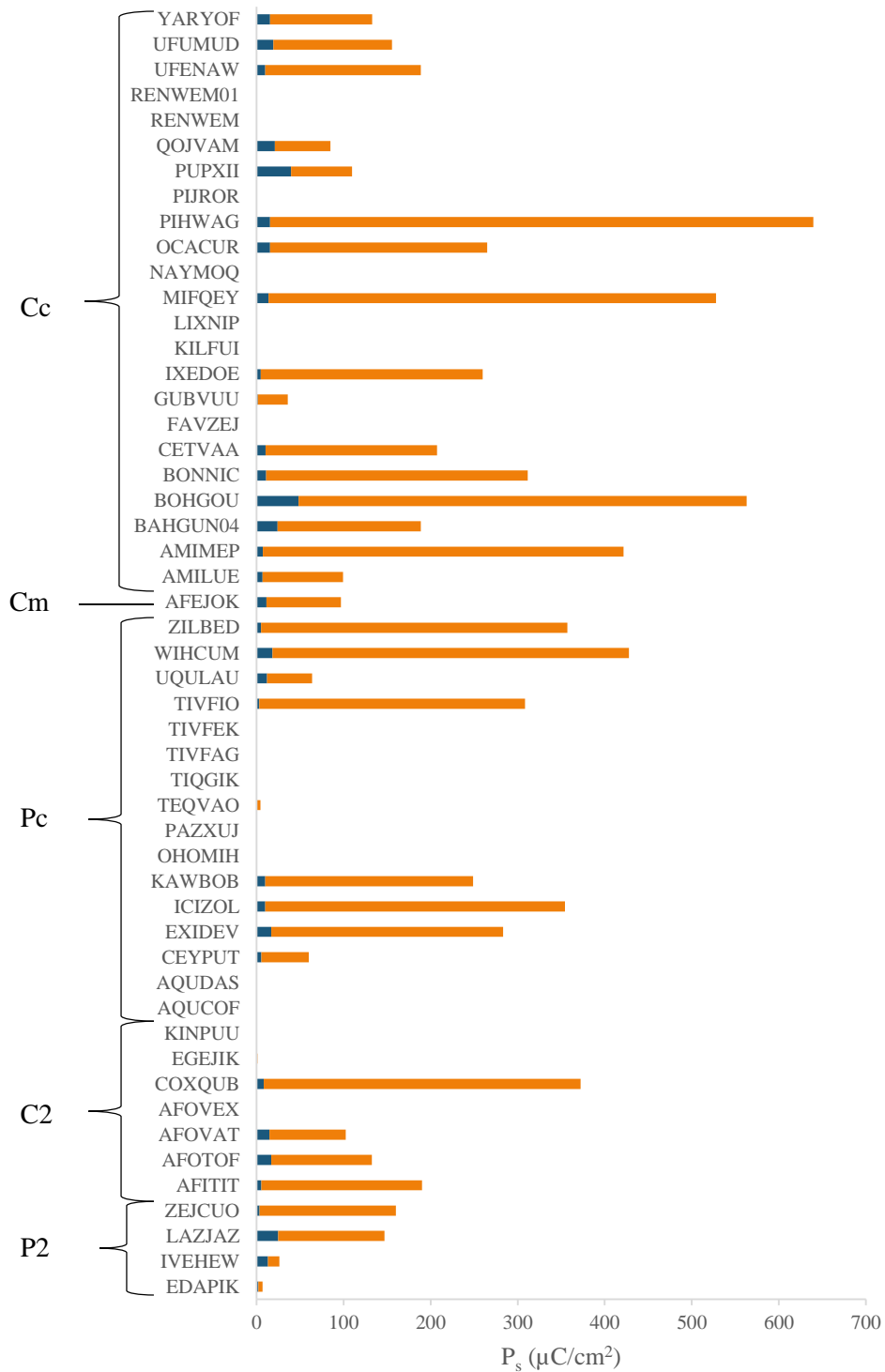
Figure 24 *Total polarization (orange) for monoclinic space groups excluding P2₁. Electronic contribution is in blue.*

Figure 25 *Total polarization (orange) for the monoclinic space group P2₁. Electronic contribution is in blue.*

Figure 26 *Total polarization (orange) for orthorhombic space groups excluding Pna2₁. Electronic contribution is in blue.*

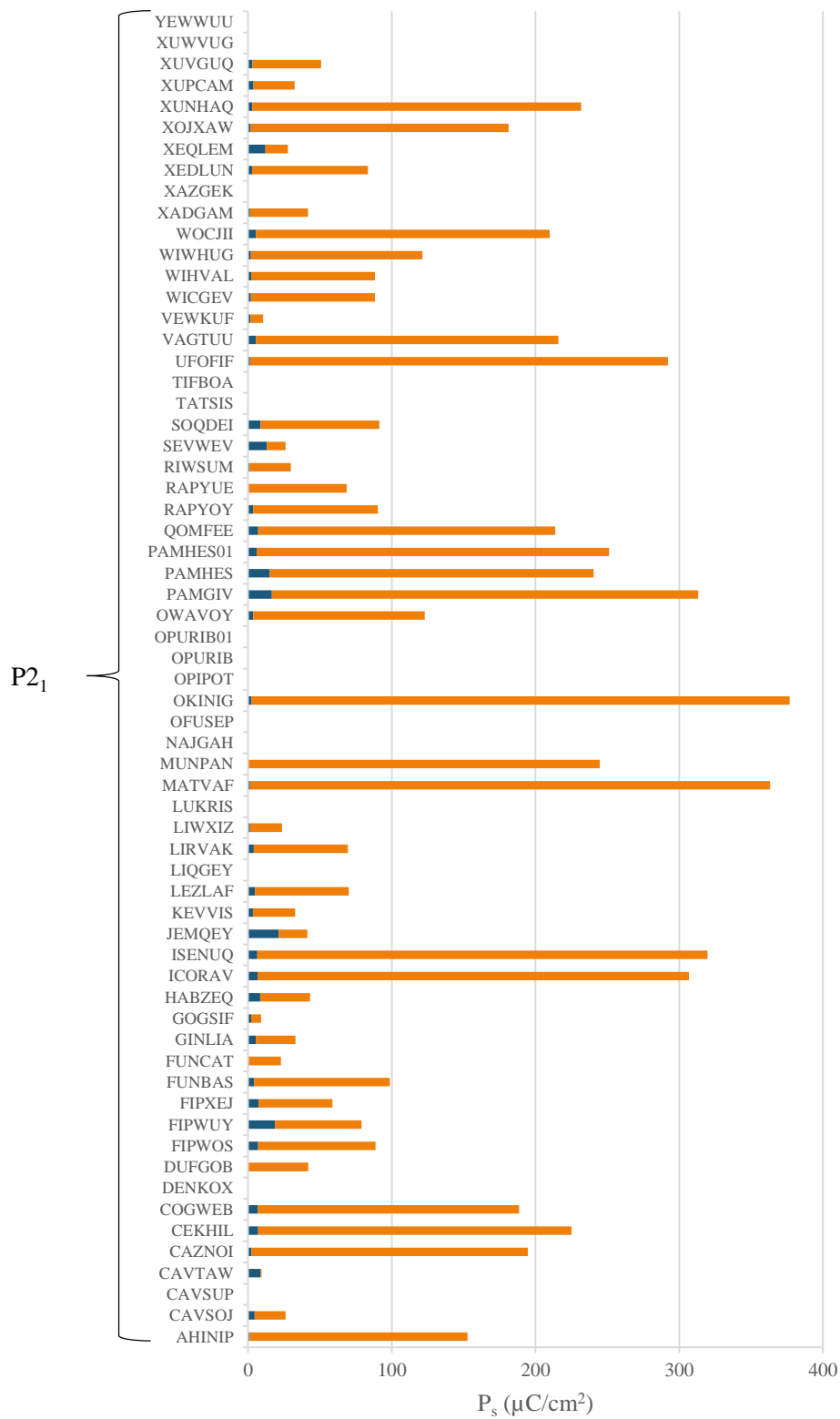*Figure 27* *Total polarization (orange) for the tetragonal space groups. Electronic contribution is in blue.*

Figure 28 *Total polarization (orange) for the trigonal space groups. Electronic contribution is in blue.*

Figure 29 *Total polarization (orange) for the hexagonal space groups. Electronic contribution is in blue.*
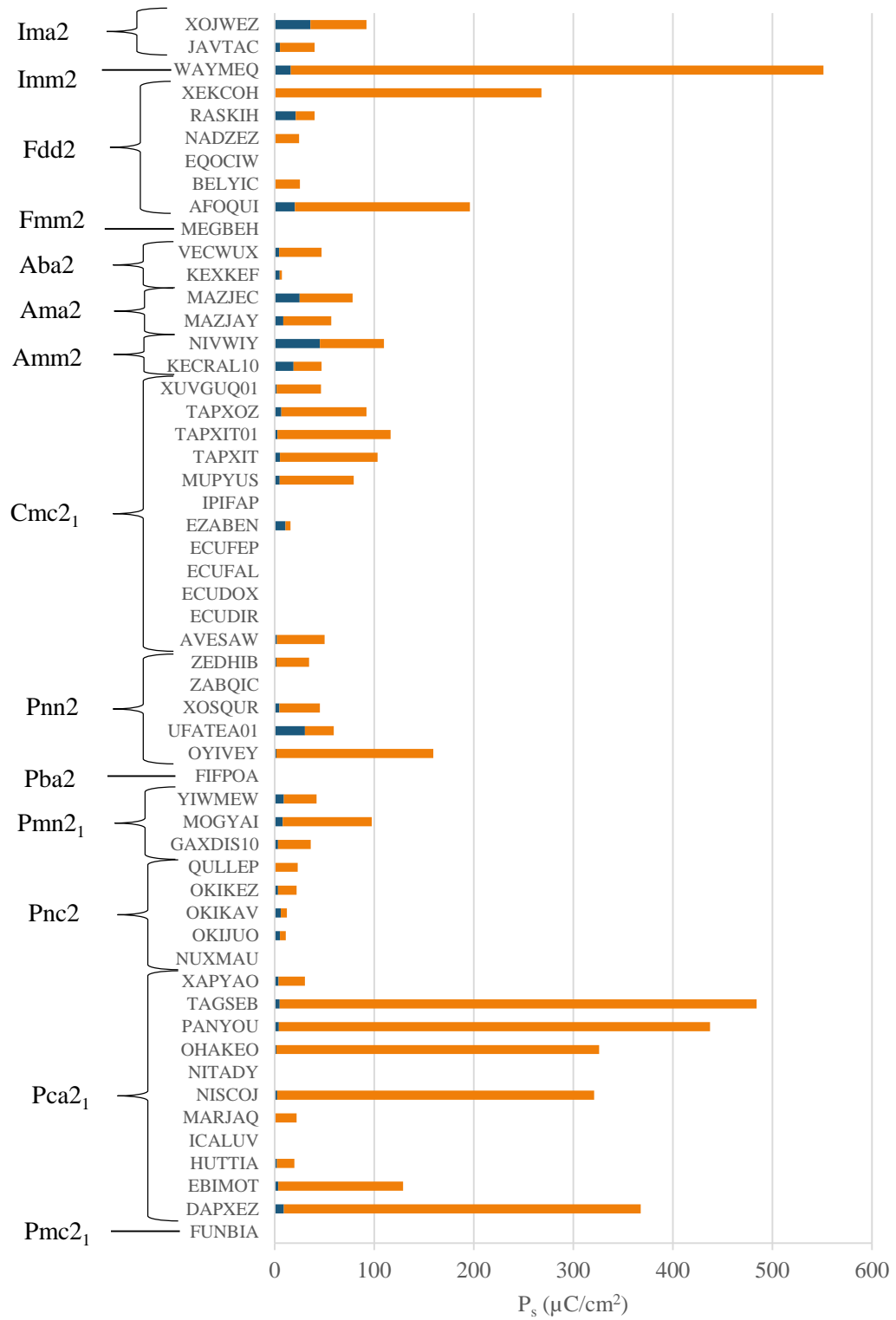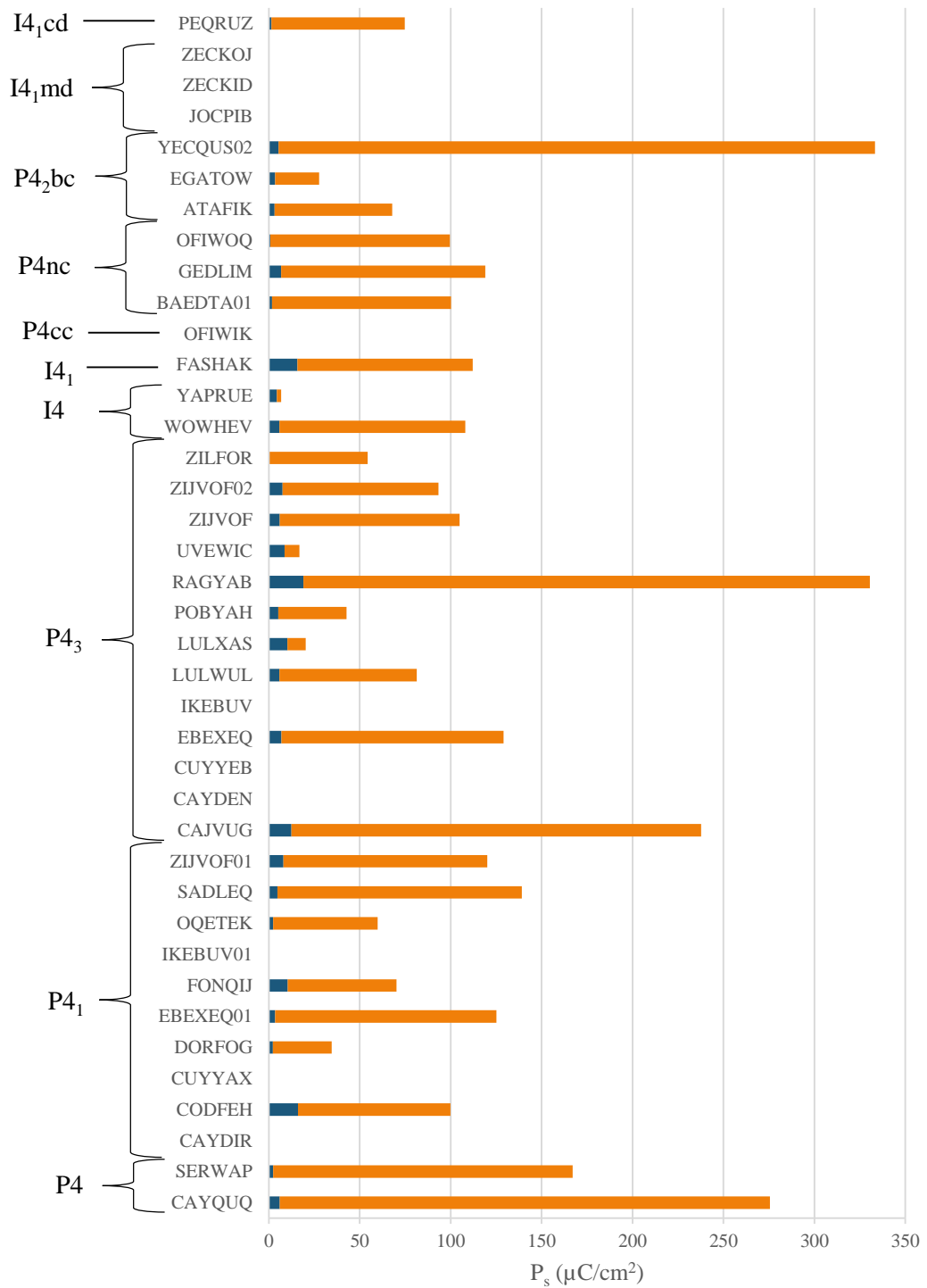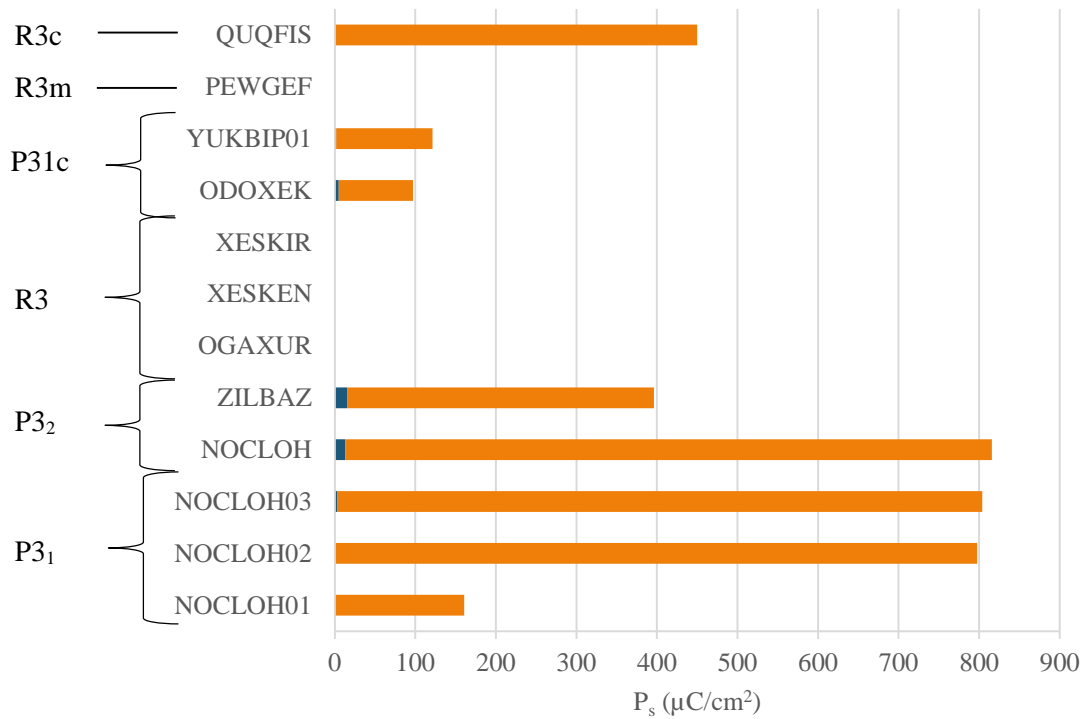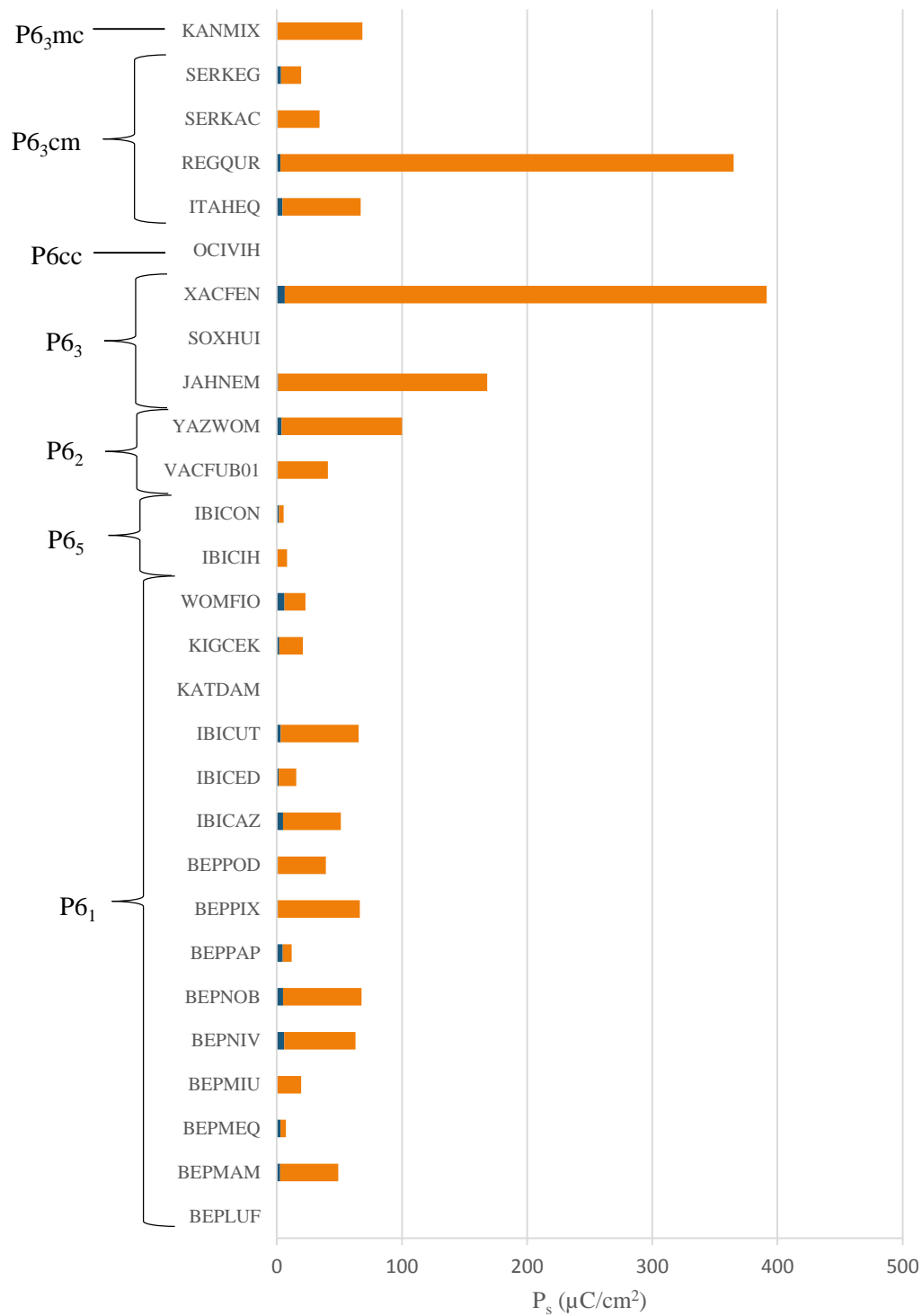
REFERENCES

1. Nathan, A., et al., *Flexible electronics: The next ubiquitous platform.* Proceedings of the IEEE, 2012. **100**: p. 1486-1517.

2. Chikazumi, S., *Physics of ferromagnetism.* 2nd Edition ed. 2009, Oxford: Oxford University Press.

3. Zhang, W. and R.G. Xiong, *Ferroelectric metal-organic frameworks.* Chem Rev, 2012. **112**(2): p. 1163-95.

4. Wudl, F. and J.D. Thompson, *Buckminsterfullerene C60 and Organic Ferromagnetism* J. Phys. Chem. Solids 1992. **53**(11): p. 1449-1455.

5. Martin, L.W. and R. Ramesh, *Multiferroic and magnetoelectric heterostructures.* Acta Materialia, 2012. **60**(6-7): p. 2449-2470.

6. Eerenstein, W., N.D. Mathur, and J.F. Scott, *Multiferroic and magnetoelectric materials.* Nature, 2006. **442**(7104): p. 759-65.

7. Lines, M.E. and A.M. Glass, *Principles and Applications of Ferroelectics and Related Materials.* 1977: Oxford University Press.

8. Hippel, A.v. and R.G. Breckenridge, *High dielectric constant ceramics.* Ind. Eng. Chem., 1946. **38**(11): p. 1097-1109.

9. Sawaguchi, E., *Ferroelectricity versus Antiferroelectricity in the Solid Solutions of PbZrO3 and PbTiO3.* J. Phys. Soc. Jpn., 1953. **8**: p. 615-629.

10. Shirane, G. and A. Takeda, *Phase Transitions in Solid Solutions of PbZrO3 and PbTiO3 (I) Small Concentrations of PbTiO3.* J. Phys. Soc. Jpn., 1952. **7**: p. 5-11.

11. Nassau, K., H.J. Levinstein, and G.M. Loiacono, *Ferroelectric Lithium Niobate. 1. Growth, Domain Structure, Dislocations and Etching.* J. Phys. Chem. Solids, 1966. **27**: p. 983-988.

12. Nassau, K., H.J. Levinstein, and G.M. Loiacono, *Ferroelectric Lithium Niobate. 2. Preparation of Single Domain Crystals.* J. Phys. Chem. Solids, 1966. **27**: p. 989-996.

13. Abrahams, S.C., J.M. Reddy, and J.L. Bernstein, *Ferroelectric Lithium Niobate. 3. Single Crystal X-ray Diffraction Study at 24°C.* J. Phys. Chem. Solids, 1966. **27**: p. 997-1012.

14. Abrahams, S.C., W.C. Hamilton, and J.M. Reddy, *Ferroelectric Lithium Niobate. 4. Single Crystal Neutron Diffraction Study at 24°C.* J. Phys. Chem. Solids, 1966. **27**: p. 1013-1018.

15. Abrahams, S.C., H.J. Levinstein, and J.M. Reddy, *Ferroelectric Lithium Niobate. 5. Polycrystal X-ray Diffraction Study between 24°C and 1200°C.* J. Phys. Chem. Solids, 1966. **27**: p. 1019-1026.

16. Loidl, A., H.v. Loehneysen, and G.M. Kalvius, *Multiferroics.* Journal of Physics: Condensed Matter, 2008. **20**(43): p. 430301.

17. Scott, J.K., *Multiferroic memories.* Nature materials, 2007. **6**: p. 256-257.

18. Cornia, A., et al., *Manganese(III) formate: A three-dimensional framework that traps carbon dioxide molecules.* Angewandte Chemie - International Edition, 1999. **38**(12): p. 1780-1782.

19. Czaja, A.U., N. Trukhan, and U. Muller, *Industrial applications of metal-organic frameworks.* Chem Soc Rev, 2009. **38**(5): p. 1284-93.

20. Lee, J., et al., *Metal-organic framework materials as catalysts.* Chem Soc Rev, 2009. **38**(5): p. 1450-9.

21. Chung, Y.G., et al., *Computation-Ready, Experimental Metal–Organic Frameworks: A Tool To Enable High-Throughput Screening of Nanoporous Crystals.* Chemistry of Materials, 2014. **26**(21): p. 6185-6192.

22. Valasek, J., *Piezo-Electric and Allied Phenomena in Rochelle Salt.* Physical Review, 1921. **17**(4): p. 475-481.

23. Shieh, J., et al., *Hysteresis behaviors of barium titanate single crystals based on the operation of multiple 90° switching systems.* Materials Science and Engineering: B, 2009. **161**(1-3): p. 50-54.

24. Wang, X.-Y., Z.-M. Wang, and S. Gao, *Constructing magnetic molecular solids by employing three-atom ligands as bridges.* Chem. Commun., 2008(3): p. 281-294.

25. Férey, G., *Nanoporous materials: A selective magnetic sponge.* Nature materials, 2003. **2**(3): p. 136-137.

26. Matsuo, T.K., Y.; Suga, H.; Seki, S., *Heat capacities of copper(II) formate tetrahydrate and tetradeuterate: A comparative study of phase transitions in layer hydrate crystals.* J. Phys. Chem. Solids, 1976. **37**: p. 499-506.

27. Wang, Z., et al., *Mn3(HCOO)6: a 3D porous magnet of diamond framework with nodes of Mn-centered MnMn4 tetrahedron and guest-modulated ordering temperature.* Chemical Communications, 2004. **3**(4): p. 416-7.

28. Jain, P., et al., *Order− Disorder Antiferroelectric Phase Transition in a Hybrid Inorganic− Organic Framework with the Perovskite Architecture.* J. Amer. Chem. Soc., 2008. **130**(32): p. 10450-10451.

29.   Jain, P., et al., *Multiferroic behavior associated with an order-disorder hydrogen bonding transition in metal-organic frameworks (MOFs) with the Perovskite ABX3 Architecture.* J. Amer. Chem. Soc., 2009. **131**(38): p. 13625-13627.

30.   Di Sante, D., et al., *Tuning the ferroelectric polarization in a multiferroic metal-organic framework.* J Am Chem Soc, 2013. **135**(48): p. 18126-30.

31.   Kamba, S., et al., *Study of the phase transition in lithium ammonium tartrate monohydrate (LAT) by means of infrared and Raman spectroscopy.* Journal of Physics: Condensed Matter, 1996. **8**: p. 8669-8679.

32.   Pepinsky, R., et al., *Ferroelectricity in Glycine Silver Nitrate.* Physical Review, 1957. **107**(6): p. 1538-1539.

33.   Choudhury, R.R., et al., *Structural phase transition in ferroelectric glycine silver nitrate.* Solid State Communications, 2008. **145**(7-8): p. 407-412.

34.   Pepinsky, R., K. Vedam, and Y. Okaya, *New Room-Temperature Ferroelectric.* Physical Review, 1958. **110**(6): p. 1309-1311.

35.   Rother, H.J., J. Albers, and A. Klöpperpieper, *Phase transitions, critical dielectric phenomena and hysteresis effects in betaine calcium chloride dihydrate.* Ferroelectrics, 1984. **54**: p. 107-110.

36.   Sholl, D.S. and J. Steckel, *Density functional theory a practical introduction.* 2009: John Wiley & Sons.

37.   Kresse, G. and J. Furthmuller, *Efficiency of ab-initio total energy calculations for metals and semiconductors using a plane-wave basis set.* Comput. Mat. Sci., 1996. **6**(15).

38.   Kresse, G. and J. Furthmuller, *Efficient iterative schemes for ab initio total-energy calculations using a plane-wave basis set.* Phys. Rev. B, 1996. **54**(16).

39.   Kresse, G. and J. Hafner, *Ab initiomolecular dynamics for liquid metals.* Physical Review B, 1993. **47**(1): p. 558-561.

40.   Kresse, G. and J. Hafner, *Ab initiomolecular-dynamics simulation of the liquid-metal–amorphous-semiconductor transition in germanium.* Physical Review B, 1994. **49**(20): p. 14251-14269.

41.   Perdew, J.P., K. Burke, and M. Ernzerhof, *Generalized Gradient Approximation Made Simple.* Phys. Rev. Lett., 1996. **77**(18): p. 3865.

42.   Perdew, J.P., K. Burke, and M. Ernzerhof, *Erratum: Generalized Gradient Approximation Made Simple.* Phys. Rev. Lett., 1997. **78**(7): p. 1396.

43.   Nye, J.F., *Physical Properties of Crystals.* 1957, Oxford: Clarendon Press.

44.   Borchardt-Ott, W., *Crystallography*. 2nd ed. 1995: Springer.

45.   King-Smith, R.D. and D. Vanderbilt, *Theory of polarization of crystalline solids.* Physical Review B, 1993. **47**(3): p. 1651-1654.

46.   Resta, R., *Theory of the electronic polarization in crystals.* Ferroelectrics, 1992. **136**(1): p. 51-55.

47.   Resta, R., *Macroscopic polarization in crystalline dielectrics: the geometric phase approach.* Reviews of Modern Physics, 1994. **66**(3): p. 899-915.

48.   Vanderbilt, D. and R.D. King-Smith, *Electric polarization as a bulk quantity and its relation to surface charge.* Physical Review B, 1993. **48**(7): p. 4442-4455.

49.   Vanderbilt, D. and R.D. King-Smith, *Electronic polarization in the ultrasoft pseudopotential formalism.* 1998. p. 1-6.

50.   Resta, R., *Berry Phase in Electronic Wavefunctions*. 1996.

51.   Kroumova, E., et al., *PSEUDO: a program for a pseudosymmetry search.* Journal of Applied Crystallography, 2001. **34**(6): p. 783-784.

52.   Capillas, C., M.I. Aroyo, and J.M. Perez-Mato, *Methods for pseudosymmetry evaluation: a comparison between the atomic displacements and electron density approaches.* Z. Krist., 2005. **220**: p. 691-699.

53.   Capillas, C., et al., *A new computer tool at the Bilbao Crystallographic Server to detect and characterize pseudosymmetry.* Z. Krist., 2011. **226**(2): p. 186-196.

54.   Aroyo, M.I., et al., *Bilbao Crystallographic Server II: Representations of crystallographic point groups and space groups".* Acta Cryst., 2006. **A62**: p. 115-128.

55.   Aroyo, M.I., et al., *Bilbao Crystallographic Server I: Databases and crystallographic computing programs.* Z. Krist., 2006. **221**(1): p. 15-27.

56.   Aroyo, M.I., et al., *Crystallography online: Bilbao Crystallographic Server.* Bulg. Chem. Commun., 2011. **43**(2): p. 183-197.

57.   *Pseudosymmetry Search Tutorial*.

58.   Jonsson, H., G. Mills, and K.W. Jacobsen, *Nudged Elastic Band Method for Finding Minimum Energy Paths of Transitions*, in *Classical and Quantum Dynamics in Condensed Phase Simulations*, B.J. Berne, G. Ciccotti, and D.F. Coker, Editors. 1998, World Scientific.

59. Mills, G., H. Jonsson, and G.K. Schenter, *Reversible work transition state theory: application to dissociative adsorption of hydrogen.* Surface Science, 1995. **324**: p. 305-337.

60. Sheppard, D., R. Terrell, and G. Henkelman, *Optimization methods for finding minimum energy paths.* J Chem Phys, 2008. **128**(13): p. 134106.

61. Henkelman, G., B.P. Uberuaga, and H. Jónsson, *A climbing image nudged elastic band method for finding saddle points and minimum energy paths.* The Journal of Chemical Physics, 2000. **113**(22): p. 9901.

62. Rabe, K.M., C.H. Ahn, and J.-M. Triscone, *Physics of Ferroelectrics: A Modern Perspective*, in *Topics in Applied Physics*. 2007, Springer-Verlag Berlin Heidelberg.

63. Gierke, T.D., H.L. Tigelaar, and W.H. Flygare, *Calculation of Molecular Electric Dipole and Quadrupole Moments.* J Am Chem Soc, 1972. **94**(2): p. 330-8.

64. Wang, Z., et al., *Anionic NaCl-type frameworks of [Mn(II)(HCOO)(3)(-)], templated by alkylammonium, exhibit weak ferromagnetism.* Dalton Trans, 2004(15): p. 2209-16.

65. Takeda, K. and K. Kawasaki, *Magnetism and Phase Transition in Two-Dimensional Lattices; M(HCOO)2·2H2O (M; Mn, Fe, Ni, Co).* J. Phys. Soc. Jpn., 1971. **31**(4): p. 1026-1036.

66. Pierce, R.D. and S.A. Friedberg, *Heat Capacities of Fe(HCOO)2·2H2O and Ni(HCOO)2·2H2O between 1.4 and 20 °K.* Physical Review B, 1971. **3**(3): p. 934-942.

67. Pierce, R.D. and S.A. Friedberg, *Heat Capacity of Mn(HCOO)2·2H2O between 1.4 and 20°K.* Physical Review, 1968. **165**(2): p. 680-687.

68. Skalyo, J., G. Shirane, and S.A. Friedberg, *Two-Dimensional Antiferromagnetism in Mn(HCOO)2·2H2O.* Physical Review, 1969. **188**(2): p. 1037-1041.

69. Hoy, G.R., et al., *Inequivalent Magnetic Ions in Dihydrated Formates of Fe+ + and Ni+ +.* Journal of Applied Physics, 1965. **36**(3): p. 936.

70. Flippen, R.B. and S.A. Friedberg, *Low-Temperature Magnetic Susceptibilities of Some Hydrated Formates of Cu++ and Mn++.* The Journal of Chemical Physics, 1963. **38**(11): p. 2652.

71. Kobayashi, H. and T. Haseda, *The Magnetic Properties of Cupric Formate Tetrahydrate at Low Temperatures.* J. Phys. Soc. Jpn., 1963. **18**: p. 541-550.

72.   MARTIN, R.L. and H. WATERMAN, *Magnetic Studies with Copper(II) Salts. Part IV. Remarkable Magnetic Behaviour of Copper(II) Formate and its Hydrates.* J. Chem. Soc., 1959: p. 1359-1370.

73.   Kageyama, H., et al., *Weak ferrimagnetism, compensation point, and magnetization reversal inNi(HCOO)2·2H2O.* Physical Review B, 2003. **67**(22).

74.   Romero, S., A. Mossett, and J.C. Trombe, *A new family of lanthanide oxalate carbonate, [Ln(H2O)]2(C2O4)(CO3)2 with Ln = Eu...Ho, presenting a relatively open framework.* Eur. J. Solid State Inorg. Chem., 1997. **34**(2): p. 209-219.

75.   Xie, Y.-M., et al., *New Ferroelectric and Nonlinear Optical Porous Coordination Polymer Constructed from a Rare (CuBr)∞ Castellated Chain.* Crystal Growth & Design, 2008. **8**(11): p. 3914-3916.

76.   Cortijo, M., et al., *Hybrid Polyfunctional Systems Based on Nickel(II) Isonicotinate.* European Journal of Inorganic Chemistry, 2013. **2013**(14): p. 2580-2590.

77.   Wu, M., et al., *Multiferroic materials based on organic transition-metal molecular nanowires.* J Am Chem Soc, 2012. **134**(35): p. 14423-9.